Reconstruction of the deformed collision zone Between India and Asia by backward motion of lithospheric blocks

A. Replumaz
Laboratoire Dynamique de la Lithosphère, Université Claude Bernard-Lyon 1, Villeurbanne, France

P. Tapponnier
Laboratoire de Tectonique, Mécanique de la Lithosphère, Institut de Physique du Globe de Paris, Paris, France

Received 5 June 2001; revised 26 September 2002; accepted 17 December 2002; published 3 June 2003.

[1] On the basis of a synthesis of tectonic data available on the India-Asia collision, we present a first attempt to reconstruct the evolution of the collision zone. Assuming that the deformation of the lithosphere is localized along narrow shear zones and that the interiors of mantle blocks in between remain relatively undeformed, we define block contours from the fault pattern and move back the blocks along their boundary faults. Along convergent or extensional boundaries, the crust is assumed to shorten or stretch coherently. Step-by-step, we go backward in time to finally reach the collision onset. For each time step, we find a solution compatible with the data set available and the position of the adjacent blocks for each block. The search for compatibility at the scale of the entire collision zone allows for solving the kinematics of regions with fewer data and suggests plausible scenarios for regions where data is lacking. For each step, we calculate large-scale displacement maps, and determine Euler poles for each block. For the most recent time step, the map proposed is compared to GPS motions. The deformation budget implies that extrusion absorbed ~30% of the convergence between India and Siberia during the entire collision span, but varied with time, accounting for as little as 3% or as much as 60% of this convergence at different epochs. *INDEX TERMS:* 8150 Tectonophysics: Plate boundary—general (3040); 8157 Tectonophysics: Plate motions—past (3040); 9320 Information Related to Geographic Region: Asia; 9604 Information Related to Geologic Time: Cenozoic; *KEYWORDS:* India-Asia collision, localized continental deformation

Citation: Replumaz, A., and P. Tapponnier, Reconstruction of the deformed collision zone Between India and Asia by backward motion of lithospheric blocks, *J. Geophys. Res.*, *108*(B6), 2285, doi:10.1029/2001JB000661, 2003.

1. Introduction

[2] A quantitative account of the deformation of Asia in response to India's penetration [*Molnar and Tapponnier*, 1975; *Patriat and Achache*, 1984; *Molnar et al.*, 1988] is key to understand long-term, lithospheric deformation processes in continents. In one class of models, the lithosphere is inferred to behave like a fluid, with diffuse deformation of the crust and upper mantle over broad areas [e.g., *England and Houseman*, 1986; *Vilotte et al.*, 1986; *England and Molnar*, 1997; *Holt*, 2000]. In general, the results of such models are compared a posteriori with observations.

[3] Another category of models, based on a priori geological evidence, suggests that continental deformation north of India can be described by motions of coherent blocks separated by long and relatively narrow fault zones along which most of the deformation remains localized at any given time [e.g., *Tapponnier et al.*, 1982, 1986; *Armijo et al.*, 1989; *Avouac and Tapponnier*, 1993; *Peltzer and Saucier*, 1996]. Quantitative data, particularly offset amounts and slip rates, on several of the major faults of Asia, may be used to constrain these models, which can be refined as evidence increases.

[4] Over the last decade, there has been growing support for localized strain along faults separating coherent blocks. The seismic anisotropy directions calculated by *McNamara et al.* [1994] in Tibet, for instance, are in agreement with velocity fields deduced from fault slip rates [*Lavé et al.*, 1996; *Griot et al.*, 1998]. Major discontinuities in the upper mantle anisotropy field beneath Tibet appear to be localized beneath faults, suggesting that they may extend to the base of the lithosphere [*Griot et al.*, 1998]. A seismic tomographic section of the Altyn Tagh fault at 90°E, reveals a steep, 40-km-wide, low-velocity zone that appears to cut through the crust and lithospheric mantle [*Wittlinger et al.*, 1998]. This narrow zone coincides with a rapid sinistral swing in the fast polarization directions of shear waves, concurrent with an increase in shear wave splitting [*Herquel et al.*, 1999], and vanishes at a depth of 150 km, implying that it reaches the base of the lithosphere. A similar sinistral shear zone, active from 35 to 16 Ma, has been documented in exhumed 20-km-wide, elongated massifs of high-grade mylonitic gneisses along the Red River fault [*Tapponnier et*

Copyright 2003 by the American Geophysical Union.
0148-0227/03/2001JB000661$09.00

al., 1990; *Leloup et al.*, 1995; *Schärer et al.*, 1990]. Average Holocene slip rates along most of the large active strike-slip faults of Asia exceed 10 mm/yr (Table 1). Several of these faults appear to have absorbed hundreds of kilometers of finite motion (Table 1). Certain blocks in between the faults, on the other hand, appear to have remained undeformed. Examples of essentially rigid blocks are the Tarim, a flat sedimentary basin with little relief between the Altyn Tagh fault and the Tian Shan, and the Ordos, a seismically quiescent zone surrounded by narrow seismogenic rifts (Figure 1). To a first order, some of the largest Tertiary faults of Asia thus seem to behave like plate boundaries.

[5] The growing body of quantitative data on finite block motions or slip rates along block boundaries (Table 1) is now sufficient that it becomes possible to retrodeform much of the area affected by the India-Asia collision using a block model on the sphere, as in plate tectonics. Previous first-order attempts have only addressed and investigated present-day strain [e.g., *Avouac and Tapponnier*, 1993; *Peltzer and Saucier*, 1996]. Here we go further to test the long-term validity of the approach since the onset of collision ~50 Ma. We go back in time by stages of a few millions of years, separated by epochs when important kinematic changes are geologically documented. The purpose of our work is to test both a geologically plausible scenario of the deformations and motions induced by the collision, and the assumption of rigid lithospheric blocks. Can blocks be considered rigid or not, and is deformation localized on fault zones or not at each stage? If certain blocks do not behave rigidly, which are they, and where? For what reasons? More generally, what is the trade-off between block motion and distributed deformation in any given area?

2. Quantitative Constraints and Reconstruction Technique

[6] Our reconstruction is a backward, step-by-step restoration of collision-induced motions assuming that strain is essentially localized along a few boundary faults separating much less deformed lithospheric blocks (Figure 1). The motions of the blocks are modeled by moving microplates on the sphere. For each time step, we propose a solution for the position of all the blocks within the collision zone, compatible with the entire data set available for this period. We finally obtain a simplified, synthetic evolution of the collision zone, all the way back to its onset, ~50 Ma.

2.1. Coherent Blocks, Block Contours, and Pattern

[7] The present-day contours of the blocks, from which we start, follow the major faults of eastern Asia (Figure 1), as mapped on the basis of detailed geomorphic and tectonic field studies and large-scale SPOT or Landsat imagery analysis [*Tapponnier and Molnar*, 1977, 1979; *Molnar and Tapponnier*, 1978; *Le Dain et al.*, 1984; *Armijo et al.*, 1986, 1989; *Peltzer et al.*, 1989; *Gaudemer et al.*, 1995; *Van Der Woerd et al.*, 1998, 2000; *Lasserre et al.*, 1999]. The largest are thrust and strike-slip faults hundreds of kilometers long. The junctions between main faults are often complicated and involve secondary faults, which we simplify and collapse into single block-bounding faults, as specified below.

[8] For a given period, a block is defined as a coherent unit, geologically and tectonically. Where the crust deforms, usually along the block's rims, it does so with a uniformity of style and trend. A block bounded primarily by strike-slip faults keeps a constant surface, and often shape, although large-scale shape change is possible. A block bounded by thrusts shrinks, generally in one direction. The corresponding deformation is usually localized on small thrusts and folds parallel to its boundaries, and may be treated as equivalent to deformation along the block rims only. At one extreme, such blocks are not rigid, but their deformation is coherent with motions along their boundaries. The same simplifying approach may be taken for blocks bounded by normal faults, which stretch predominantly in one direction. Another way to treat the problem of deformation within blocks away from their boundary is to subdivide the deforming regions into smaller blocks. The scale of the collision zone, however, and the limited amount of data available on the timing of slip on most faults make this difficult at this stage.

[9] The present-day limit between India and Asia is the thrust along the Main Himalayan front (MFT). It separates rigid India from southern Tibet. The central part of South Tibet is rifted into seven small blocks [*Armijo et al.*, 1986]. We simplify this coherent deformation and divide South Tibet into three main blocks (Figure 1). The Pakistan-Pamir block is bounded on the west by the Chaman fault, to the north by the Main Pamir Thrust and to the east by the Karakorum fault. We assume the southeastern branches of the Karakorum fault terminate into the Thakkhola graben. The Lhasa-Himalaya block is limited to the west by the Karakorum fault and to the north by the Karakorum-Jiali fault zone, taken to mark a simpler, continuous boundary at the lithospheric mantle level [*Armijo et al.*, 1989; *McCaffrey and Nábelek*, 1998]. We subdivide this block further into two smaller blocks separated by the Yadong-Gulu rift zone. Our choice of two more prominent block boundaries within South Tibet is justified by the observation that the Yadong and Thakkhola grabens are the main ones that cross the Himalayan range southward.

[10] The northern edge of the Tibet plateau is marked by the Altyn Tagh fault. As active thrusting becomes more prominent northeastward, the sizes of coherent blocks within northern Tibet decrease in that direction. The Qiangtang platform is the largest Tibetan block (Figure 1). It is cut by small normal faults [*Molnar and Tapponnier*, 1978; *Armijo et al.*, 1986] that slip at slow rates [*Yin*, 2000], and that we hence neglect to a first order. Its southern limit follows the dextral Karakorum-Jiali fault zone, the northern branch of which can be connected eastward with the Red River fault, across the Lijiang extensional pull aparts [*Armijo et al.*, 1989]. The northeast limit of Qiangtang is the Xianshui He fault, which curves southward into the Xiaojiang fault before abutting the Red River fault. The northern limit follows the Fenguo Shan thrusts [*Meyer et al.*, 1998], between the Xianshui He and the Kunlun faults, then the north branch of the Kunlun fault, to the Altyn Tagh fault. The western tip of Qiangtang is considered to be a small, independent block, the West Tibet block, separated from Qiangtang by the Gozha fault [*Peltzer et al.*, 1989]. The Songpan block is the triangular wedge between the Kunlun fault, the Longmen Shan and the Xianshui He-

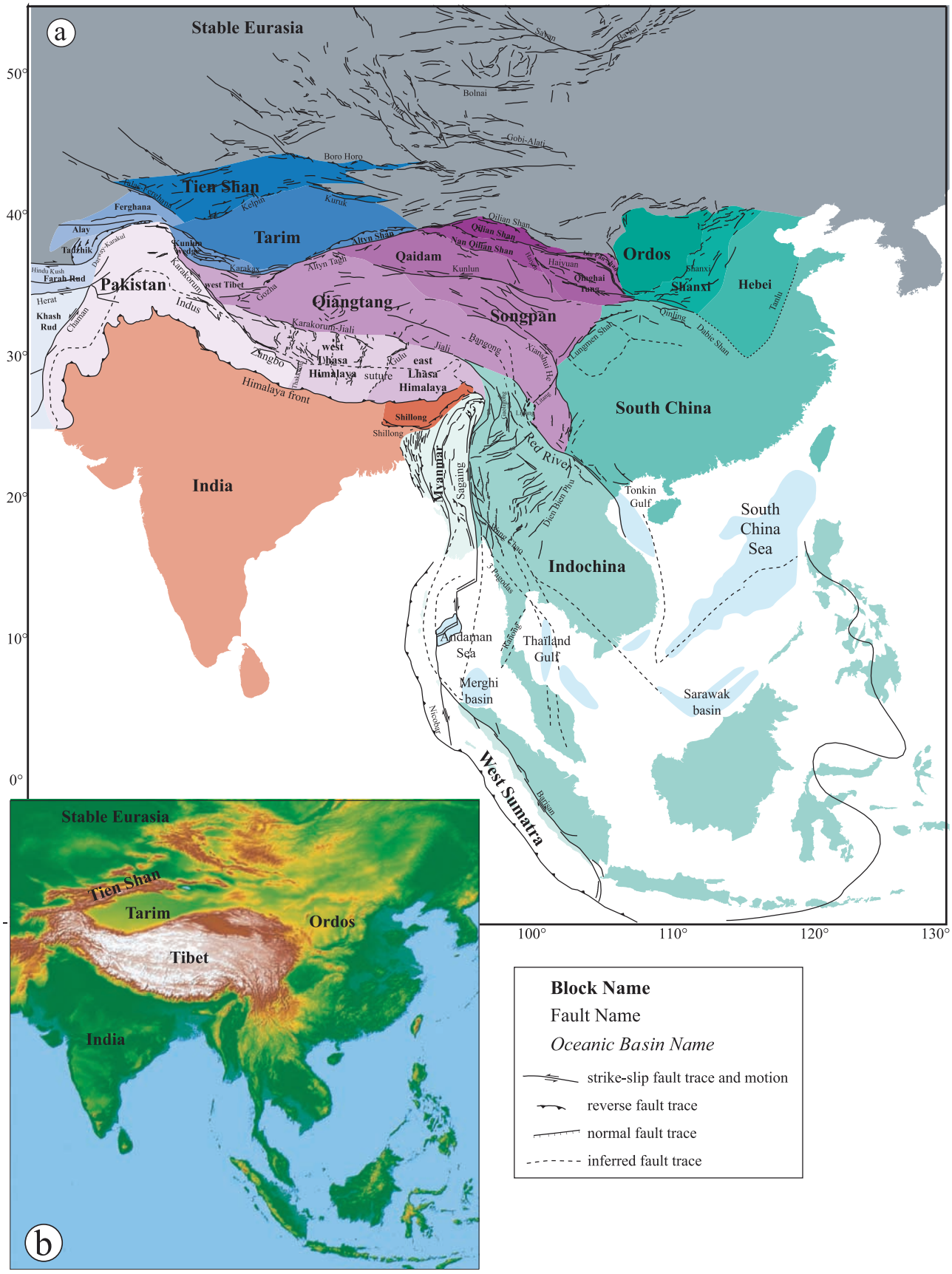


Figure 1. (a) Block contours defined from active fault map of Asia (see text). (b) Corresponding topographic map (GETOPO 30).

Table 1. Data Set Available at Each Time Step

Faults	Slip Rate, mm/yr	Total Displacement, km	Period of Activity, Ma	Reference
Altyn Tagh	30 ± 10			*Peltzer et al.* [1989]
	25 ± 5			*Mériaux* [2002]
		500		*Peltzer and Tapponnier* [1988]
Kunlun	12 ± 2			*Van Der Woerd et al.* [1998]
		150 ± 50		*Meyer et al.* [1998]
Xian Shui He	15 ± 5			*Allen et al.* [1991]
		70 ± 10		*Gaudemer et al.* [1995]
Red River Dextral	5			*Replumaz et al.* [2001]
		25		*Replumaz et al.* [2001]
			0–5	*Leloup et al.* [1995]
Red River Sinisral		700 ± 200		*Leloup et al.* [1995]
			15–30	*Briais et al.* [1993]
Karakorum	32 ± 5			*Liu* [1993]
		1000		*Peltzer and Tapponnier* [1988]
Haiyuan	12 ± 4			*Lasserre et al.* [1999]
		125		*Gaudemer et al.* [1995]
			0–10	*Jolivet* [2000]
Himalaya front	17.7 ± 2			*Bilham et al.* [1997]
	21.5 ± 1.5			*Lavé and Avouac* [2000]
		>470		*Coward and Butler* [1985]
		>530		*Ratschbacher et al.* [1994]
Talas-Ferghana	10			*Burtman et al.* [1996]
		180–250		*Burtman et al.* [1996]
Jiali	10 ± 5			*Armijo et al.* [1989]
			0–5	*Armijo et al.* [1989]
Wang Chao		160		*Lacassin et al.* [1997]
			30–40	*Lacassin et al.* [1997]
3 Pagodas		160		*Lacassin et al.* [1997]
			30–40	*Lacassin et al.* [1997]

Block	Period, Ma	Data Type	Reference
India	0–5	rotation rate	*DeMets et al.* [1994]
	5–50	rotation rate	*Patriat and Achache* [1984]
Tarim		rotation pole	*Avouac et al.* [1993]
	0–5	rotation rate	*Avouac and Tapponnier* [1993]
	≥0–15	total amount of rotation	*Avouac et al.* [1993]
Ordos	≥0–10	rotation pole and total amount of rotation	*Zhang* [1994]
Indochina	15–30	rotation rate	*Briais et al.* [1993]

Fenguo Shan boundary (Figure 1). The Qaidam block encompasses the Qaidam and Gonghe basins, between the Kunlun fault, the Nan Qilian Shan thrust and the Haiyen fault. The Qinghai Tung block is limited to the west by the Haiyen fault, to the south by the eastern continuation of the Kunlun fault, and to the northeast by the Haiyuan fault. The Nan Qilian Shan block lies between the Qaidam basin, the Haiyen fault and the western continuation of the Haiyuan fault along the Sulenan and Tanghenan Shan. The northeasternmost, smallest sliver of Tibet, the Qilian Shan block, is limited to the north by the Qilian Shan frontal thrust and to the south by the western Haiyuan fault.

[11] In this paper, we do not model deformation north of the Tian Shan, which is smaller than in regions to the south. Long-term slip rates on the largest Mongolian faults or across the Baikal rift appear to be only a few millimeters per year, even though the area has been the site of several great earthquakes since 1900 and GPS motions are significant, possibly due in part to postseismic strain [*Ritz et al.*, 1995; *Lesne et al.*, 1997]. Tertiary finite offsets in Mongolia also appear to be smaller than a few tens of kilometers. Thus the deformation absorbed north of the Tarim is assumed to be taken up chiefly by thickening of the Tian Shan. Because of coherent shortening on several thrusts along and within the range, we define a Tian Shan "block", whose limits are taken to coincide with the topographic edges of the range. The northern boundary of the Tian Shan thus marks the northeastern limit of the region investigated (Figure 1). Recent GPS results [*Shen et al.*, 2001] indeed suggest that points north of that boundary move little relative to stable Eurasia. Geologically, however, this is a rather crude simplification. Some paleomagnetic results [*Halim et al.*, 1998] imply several hundred kilometers of post-Cretaceous shortening between the Tian Shan and Siberia, and a few hundred would not be inconsistent with the present-day relief of the Altai and Sayan ranges. However, this simplification bears mostly on the total amount of shortening across Asia, hence on the age of the onset of collision, rather than on the evolution of deformation where it has been largest, between the Himalaya and the Tian Shan.

[12] The rigid Tarim block is well defined. It is covered by the flat Takla Makan desert, which lies between the active faults that bound the high mountains surrounding it (Figure 1b). Two small mountainous slivers, the Kunlun Wedge and the Altyn Shan, are squeezed between Tibet and the Tarim, due to slip partitioning. They are bounded by thrusts to the north and by the Altyn Tagh-Karakax fault to the south.

[13] In the northeastern part of the collision zone, north China may be divided into three subblocks (Figure 1). The rigid Ordos block is characterized by internal seismic quiescence, and surrounded on all sides by oblique, step-

ping rifts, clear both on the topographic and historical or instrumental seismicity maps [*Gu et al.*, 1989]. The Fen Wei rift, site of some of China's greatest historical earthquakes, is the limit between the Ordos and Shanxi blocks. The limit between the Shanxi and Hebei blocks, site of the Xingtai 1966 earthquakes [*Tapponnier and Molnar*, 1977] is also clear. Though less active, the Tanlu fault separates the Hebei plains from Shantung, the northern prong of south China, itself a well-defined, mildly seismic block. All three blocks are bounded to the south by strike-slip faults within the Qinling-Dabie range [*Peltzer et al.*, 1985] and to the north by the Hetan-Bohai fault zone.

[14] We divide Southeast Asia into four principal blocks (Figure 1). South China, bounded on the north by the Qinling-Dabie and Tanlu faults, is bounded on the west by the Longmen Shan and the Xiaojiang fault, the southernmost extension of the Xianshui He fault. The Red River fault forms the boundary between south China and Indochina. The northwestern tip of Indochina is separated from Qiangtang by the eastern extension of the Jiali fault. The western limit of Indochina is the Sagaing fault. Toward the south, this limit continues through the Mid-Andaman spreading center and joins the Barisan fault north of Sumatra. This latter fault separates Indochina and Sunda from the West Sumatra forearc sliver. Though this sliver may be subdivided into three smaller blocks by transtensive transfer of dextral slip to the subduction interface [*Sieh and Natawidjaja*, 2000], we consider it a single block. The Sagaing fault-Andaman rift on one side and the active thrusts and folds of the Arakan Yoma range and Andaman-Nicobar arc on the other [*Le Dain et al.*, 1984] isolate another sliver or microplate, the Myanmar block [*Guzman-Speziale and Ni*, 1996]. The Nicobar fault, a bathymetric and seismic feature whose key role will be demonstrated by our reconstruction, separates this block from West Sumatra. Between Myanmar and the eastern Himalaya, one small thrust sliver, the Shillong block, is caught between the HFT and the Dauki thrust, which separates it from India.

[15] In the northwestern part of the collision zone, Afghanistan and western central Asia may be subdivided in five principal blocks (Figure 1). The northernmost block, the Ferghana block, is limited to the north by the Talas-Ferghana fault, to the west by the Chatkal thrusts and to the south by the Alay thrust. The Alay block is a thrust sliver that corresponds to the Alay range. The Tadjik block coincides roughly with the Tadjik basin, between the Alay and Hindu Kush ranges and the sinistral Darwaz-Karakul fault to the east. The Farah Rud block is a thrust sliver comparable to the Alay. The Khash Rud block is limited by the conjugate Herat and Chaman strike-slip faults, and to the west and south, by thrusts along the Lut block and Makran, respectively.

2.2. Time Steps

[16] Our reconstruction is performed step by step. The timing of each step is constrained by epochs known to correspond to major changes of deformation regime during the collision, particularly on the great strike-slip faults of eastern Asia. There are only a few time steps, because only the few changes that are sufficiently well characterized can be taken into account. Though the time steps chosen might appear to be artificially sharp, they correspond to the best documented, most radical changes in the collision history. Recall that the age of the onset of motion on several faults is poorly known, even for major ones such as the Kunlun or Altyn Tagh faults. Because chronological evidence along the main faults becomes rarer as one goes back in time, the steps also become longer.

[17] The youngest deformation change that is fairly well documented appears to be the dextral reactivation of the Red River fault around 5 Ma [*Leloup et al.*, 1995; *Replumaz et al.*, 2001]. We assume that slip rates on the main faults of Asia have not changed much since that time, as suggested by the uniformity of tectonic styles and movements from the Pliocene to the present in most areas. This first step is thus taken to be a simple extension of the present-day kinematics, and our results may be compared with those of instantaneous deformation models.

[18] The second time step corresponds to the likely activation of the Haiyuan fault, around 10 Ma. This age is inferred both from apatite fission tracks that indicate mid-Miocene exhumation of uplifted granites along the fault [*Jolivet*, 2000; *Lasserre*, 2000], and from the extrapolation of the now well constrained slip rate (12 ± 4 mm/yr [*Lasserre et al.*, 1999]) to the time needed to reach the total Tertiary offset on the fault, which significantly exceeds the $\sim$100 km offset of the Yellow river [*Gaudemer et al.*, 1995; *Lasserre et al.*, 1999; *Lasserre*, 2000]. The third step corresponds to the end of left-lateral motion along the Red River-Ailao Shan shear zone, which is well known to have occurred about 15 Ma, as seafloor spreading ceased completely in the South China Sea [*Briais et al.*, 1993; *Leloup et al.*, 1995]. The fourth step is taken to be around 30 Ma ago, roughly coeval with the onset of seafloor spreading in the South China Sea ($\sim$32 Ma [*Briais et al.*, 1993]), and following shortly the end of motion on the Wang Chao and 3 Pagodas faults (between 30 and 40 Ma [*Lacassin et al.*, 1997]). The fifth step corresponds roughly to the activation of the Wang Chao and 3 Pagodas faults ($\sim$40 Ma [*Lacassin et al.*, 1997]). A final step is used to discuss the age of the onset of collision, between 45 and 60 Ma [e.g., *Patriat and Achache*, 1984; *Dewey et al.*, 1989; *Jaeger et al.*, 1989]. Clearly, the time steps chosen, somewhat arbitrarily rounded up to coincide with simple numbers, are likely to change as more chronological data becomes available.

2.3. Block Motion Data Set

[19] Previous large-scale studies have yielded Euler parameters describing the motion of a few blocks, either during the whole collision span or for some time steps only. The corresponding poles and amounts of rotation are thus used as input data (Table 1). Such rotation parameters are available for only four blocks. For the first stage, between 0 and 5 Ma, which is a mere extrapolation of present-day motion, we used the "instantaneous" kinematics determined for several of the blocks. For India (Table 1), we took the Nuvel-1A pole [*DeMets et al.*, 1994]. For previous stages, we used the position of India relative to Asia, as constrained by seafloor magnetic anomalies [*Patriat and Achache*, 1984]. A first-order pole position and total amount of rotation relative to Siberia were estimated for the Tarim block by *Avouac et al.* [1993] from the large-scale topography of the Tian Shan (Table 1). Thus between 0 and 5

Ma, we used for this block the instantaneous rate determined by *Avouac and Tapponnier* [1993], and adapted the rate for previous stages in keeping with the total angle of rotation. Similarly, we used the pole and total amount of rotation of the Ordos block estimated by *Zhang* [1994] from the geometry and kinematics of the faults along the grabens that surround it (Table 1). Finally, the well determined motion of Indochina between 15 and 30 Ma, which is constrained by seafloor spreading magnetic anomalies in the South China Sea [*Briais et al.*, 1993] and corroborated by structural and paleomagnetic studies along the Red River fault [e.g., *Yang and Besse*, 1993; *Leloup et al.*, 1995], serves as the principal input to our reconstruction (Table 1).

[20] Otherwise, the key data input in the modeling is quantitative geological knowledge of finite amounts of slip during certain epochs along major boundaries (Table 1). Such data become rarer as time unfolds back, but are presently just enough that the modeling attempt is not critically underdetermined. They are sufficient to assess the position of most blocks well, which yields acceptable solutions for the least determined areas.

[21] For the first stage (0–5 Ma), the data set comprises mostly slip rates on most, though not all, of the large active faults of Asia, as constrained for the Holocene period with dating of geomorphic markers, which we extrapolate back to 5 Ma (Table 1). We chose to use Holocene rates rather than decadal motions derived from GPS studies [e.g., *Chen et al.*, 2000; *Wang et al.*, 2001; *Shen et al.*, 2000; *Bendick et al.*, 2000] because it remains unclear whether such motions are representative of long-term rates [*Shen et al.*, 2001], and the density of stations is still too small in many places to assess slip rates on faults. The differences between the corresponding displacement fields will be discussed.

[22] For stages prior to 5 Ma, the data set is reduced and becomes less homogeneous. Nevertheless, for lack of evidence to the contrary, slip rates on large faults are assumed to remain roughly constant over their life spans. Similarly, the senses of slip on most faults remain constant unless documented otherwise, such as for the Red River fault. Though qualitative, such constraints are strong ones. The total offset on a given fault, where known, is equally important. The combined use of such information is essential for the time steps from 5 to 10 and 10 to 15 Ma, in which slip rates are not directly available but in which we assume that most faults are still playing roles comparable to those of today. Before 15 Ma, the data set comprises mostly senses and finite offsets on large faults and Euler parameters of few plate-size blocks (Table 1).

[23] Knowledge of the structure of the deformation zone also decreases going back in time. From 5 to 15 Ma, the overall geodynamic pattern is similar to the present-day pattern. Many of the major features absorbing most of the deformation remain the same. Prior to 15 Ma, on the other hand, radical changes occur in the geometry of active faults. Between 15 and 30 Ma, for instance, the largest strike-slip boundary likely becomes the left-lateral Red River fault. Its life span, total offset, and kinematics are now well known [*Peltzer and Tapponnier*, 1988; *Briais et al.*, 1993; *Leloup et al.*, 1995; *Harrison et al.*, 1996], but the full consequences of this major geodynamic change on the entire collision realm have not been explored. One first-order problem to solve for this epoch is to redefine the main fault pattern in Tibet, which is not known [e.g., *Tapponnier et al.*, 1986]. Accordingly, the reconstruction prior to 15 Ma becomes more schematic. Prior to 30 Ma, the block motions depicted should be mostly considered to be working hypotheses.

2.4. Reconstruction Technique

[24] Each time step of retrodeformation of the lithosphere is divided into three stages: rigid rotation, boundary deformation by contour adjustment, and revision of the fault pattern.

[25] In the first stage, the blocks, considered rigid, are moved on the sphere without any shape change (Figure 2). The block contours are digitized and the plate tectonics software Terra Mobilis (C. R. Denham and C. R. Scotese, unpublished report, 1989) is used to calculate Euler poles corresponding to block motions performed according to the data set available for each period. The best fitting positions of the whole set of blocks are thus adjusted. This search for overall compatibility at the scale of the whole deformation zone is a key aspect of our approach. It is done by trial and error, which permits to test the consequences of several hypotheses. The resulting Euler parameters for the rotation of each block in the reference frame of stable Eurasia are listed in Table 2.

[26] The result of this first stage of retrodeformation is a new map of block positions after rotation on the sphere (Figures 3a to 8a). Since the reconstruction is done backward, gaps form along shortening block boundaries, and overlaps along extensional ones (Figures 2a and 2b). This new map is projected on the initial map to assess the overall displacement field (Figures 3b to 8b). The surface misfits between block contours in their new and initial positions are also measured, particularly where shortening or extension is known to have occurred, to estimate the surface change related to either. There can be regions with gaps or overlaps that do not correspond to observed shortening or extension, however. Such misfits signal incompatible block motions (Figure 2c). A common example is that of motions near the junction of curved strike-slip faults with opposite senses and conjugate trends. In the case shown on Figure 2c, for instance, bending of the middle block would be needed to minimize the gap and overlap, which reflects the fact that such a block cannot be moved without internal deformation. The existence, number and persistence of incompatibility zones provide a measure of where and by how much the rigidity assumption fails.

[27] For each time step, the second stage consists in restoring the continuity of the block pattern, in order to continue the backward reconstruction. New block contours that eliminate surface misfits are drawn on the map resulting from the first stage. This corresponds mostly to backward restoration of crustal thickening or thinning, along block boundaries where thrusting or normal faulting occurs.

[28] The third stage consists in bringing up-to-date the fault pattern that will be activated in the next time step. Changes in this pattern imply additional changes in the block contours. The new boundary fault network is drawn on the map resulting from the second stage. In the following, step-by-step description of the backward reconstruction, we show the second and third stages together for each time step (Figures 3c to 8c). For each stage, the corresponding displacement field, relative to stable Eurasia, calculated

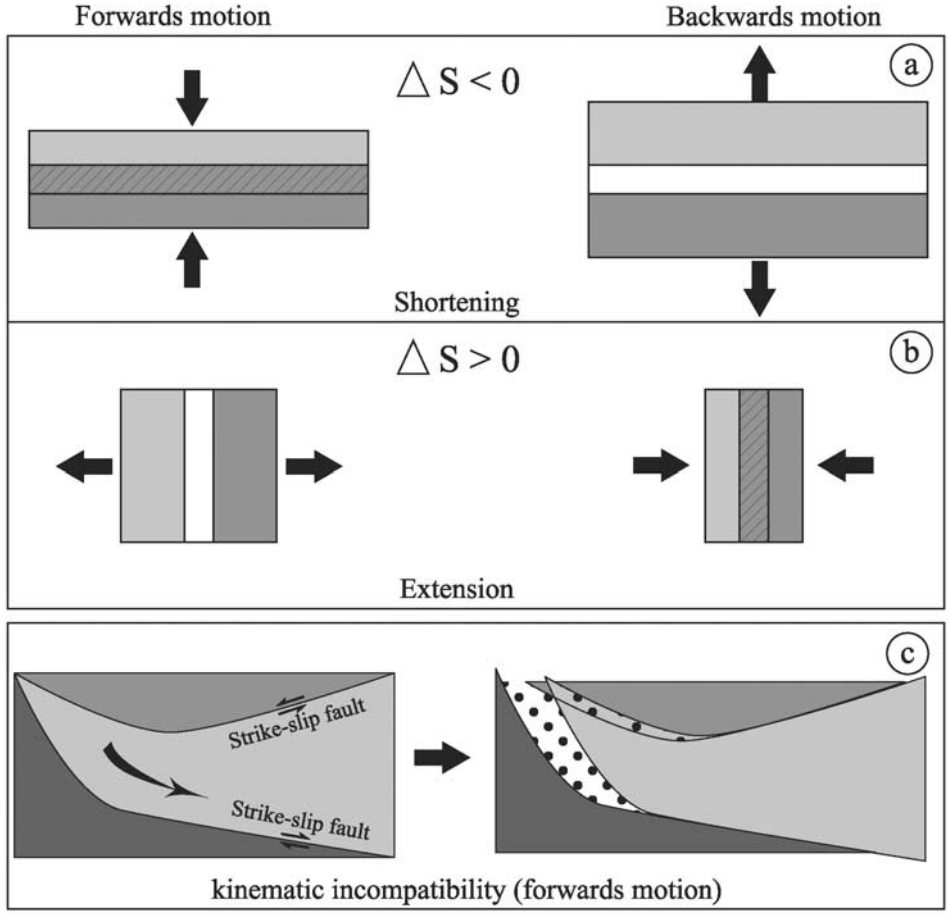


Figure 2. Type of deformation observed for a backwards reconstruction: (a) gaps form along shortening block boundaries, (b) overlaps along extensional ones, and (c) unobserved deformation if rigid block assumption failed, as near the junction of curved strike-slip faults with opposite senses and conjugate trends.

from the Euler poles determined in the reconstruction, is also shown (Figures 3b to 8b).

3. Results of Step-by-Step Retrodeformation of Block Mosaic Between 0 and 50 Ma

[29] In the following discussion, we will mostly refer to blocks moving backward in time, as they do in retrodeformation steps, and thus refer to Figures 3a to 8a. To avoid confusion, when discussing forward block motion, we will refer instead to Figures 3b to 8b.

3.1. Time Step 0–5 Ma

[30] For this step, we simply extrapolate the present-day kinematics. The resulting positions of the blocks after rotation on the sphere are shown on Figure 3a. India moves back south ~250 km. The Himalayan gap corresponds to ~100 km of north-south convergence absorbed by the Himalayan frontal thrust. The equivalent average thrust rate is ~20 mm/yr, compatible with tectonic and GPS estimates (20 ± 10 mm/yr [*Armijo et al.*, 1986]; 18 ± 7 mm/yr [*Molnar and Lyon-Caen*, 1989]; 17.5 ± 2 mm/yr [*Bilham et al.*, 1997]; 21.5 ± 1.5 mm/yr [*Lavé and Avouac*, 2000]). There is a slight eastward increase of shortening along the Himalayan front, which may account for the greater elevation of the range in Nepal. In the easternmost Himalaya, the shortening rate decreases again because of the presence of an additional thrust, the Dauki thrust, south of the Shillong block. The overlap along the Gulu boundary corresponds to ~20 km of distributed east-west extension in south Tibet [*Armijo et al.*, 1986], absorbing part of the right lateral shear between Qiangtang and South Tibet blocks [*Avouac*, 1991]. The other overlap (~4.5 km) along the Thakkhola boundary is equal to the amount of dextral slip during this period on the southernmost stretch Karakorum fault. Recall that our model is a simplification of reality. Clearly the amount of extension along the Thakkhola is much less. Slip along the Karakorum fault must thus be transferred to other faults, implying more distributed extension, in agreement with recent GPS results [*Wang et al.*, 2001].

[31] Crustal slivers in north central Tibet move back southwestward, accommodating both sinistral strike-slip and overthrusting, which are large in this region. Such motions fit the long-term slip rate along the Kunlun (~12 mm/yr [*Van Der Woerd et al.*, 1998]), Xianshui He (~15 mm/yr [*Allen et al.*, 1991]), and Haiyuan (12 mm/yr [*Gaudemer et al.*, 1995; *Lasserre et al.*, 1999]) faults. They also fit the

Table 2. Step-by-Step Euler Poles, Block Motions Relative to Siberia

Block	Latitude Pole	Longitude Pole	Angle of Rotation	References
		Time Step 0–5 Ma, 25 Blocks		
India	24.4	17.7	−2.5	*DeMets et al.* [1994]
Tarim	43.5	95.7	3.2	*Avouac and Tapponnier* [1993]
Ordos	42.2	117	−2.5	*Zhang* [1994]
South China	6.5	101.4	1.6	
Hebei	58.3	139.8	−1.5	
Shanxi	57.2	133.1	−1.2	
Qilian	32.3	102.3	6.3	
Qiangtang	20.5	99.5	6.7	
Sungpan	16.6	105.2	2.8	
Nan Qilian	30.8	103.2	5.4	
Qinghai Tung	31.9	103.1	5.5	
Qaidam	30	105.6	4.7	
East Lhasa-Himalaya	30.7	−16.3	−1.3	
West Lhasa-Himalaya	34.3	9.7	−1.4	
West Tibet	38.3	74.7	−14.3	
Kunlun wedge	39.8	105.5	2.9	
Altyn Shan	43.3	96.7	4.5	
Ferghana	32.6	66.2	−2.2	
Alay	37.7	67	−4.4	
Tadjik	37.2	69.1	−13.5	
Pakistan	−0.4	154.2	1.3	
Shillong	−16.9	174.3	2.1	
Myanmar	15.9	124.8	4.2	
Indochina	18.2	104.3	3.3	
West Sumatra	21.3	111.2	3.3	
		Time Step 5–10 Ma, 21 Blocks		
India	−11.5	−133.6	5.1	*Patriat and Achache* [1984]
Tarim	43.5	95.7	2.5	*Avouac and Tapponnier* [1993]
Ordos	42.2	117	−2.5	*Zhang* [1994]
Southeast Asia	10.5	120.2	2	
Hebei	10.6	101.1	1.3	
Shanxi	57.2	133.1	−1.2	
Qiling	23.6	106.7	3.8	
Qilian	32.5	101.3	3.3	
Qiangtang	−16.9	120.4	2	
Sungpan	−5.2	122.7	1.9	
Nan Qilian	31.1	101.9	3.1	
Qinghai Tung	29.9	102	2.3	
Qaidam	30.4	100.4	6	
Himalaya	−0.1	164.3	1.5	
Kunlun wedge	27.8	121.5	1.2	
Altyn Shan	39.3	93.8	7.3	
Ferghana	32.6	66.2	−2.2	
Alay	37.7	67	−4.4	
Tadjik	37.2	69.1	−13.5	
Myanmar	5.4	39.7	−4.6	
West Sumatra	12.9	127.9	2.2	
		Time Step 10–15 Ma, 14 Blocks		
India	21.5	27.7	−2.7	*Patriat and Achache* [1984]
Tarim	43.5	95.7	1.3	*Avouac and Tapponnier* [1993]
Southeast Asia	26.3	1.1	−0.6	
Qiangtang	46.5	−4.7	−1.4	
Sungpan	47.9	6.3	−1.1	
Qaidam	32.1	102.5	2.8	
Himalaya	3.9	125.6	1.8	
Kunlun wedge	33.1	86.2	8.1	
Altyn Shan	38.5	93.6	4.2	
Ferghana	36.3	68.7	−3.5	
Alay	37.5	67.7	−3.5	
Tadjik	36.1	67.5	−3.5	
Myanmar	0	180	2.2	
West Sumatra	17.2	−170.7	1.7	
		Time Step 15–30 Ma, 8 Blocks		
India	14.4	36.7	−8.5	*Patriat and Achache* [1984]
Indochina	5.3	86.2	10.7	from *Briais et al.* [1993]
Pamir	−1.8	160.5	1.4	
Pakistan	26.9	50.5	−4.8	
Sichuan	44.5	120	−0.9	
Qiangtang	57.5	81.1	−1.9	

Table 2. (continued)

Block	Latitude Pole	Longitude Pole	Angle of Rotation	References
Himalaya	22.6	52.9	−8.3	
Lhasa	3.5	91.6	10.4	
		Time Step 30–40 Ma, 5 Blocks		
India	17.3	42.3	−7.7	*Patriat and Achache* [1984]
North Indochina	0.2	98.2	4.8	
Central Indochina	−3.9	100.3	9.6	
South Indochina	−18.6	106.4	6	
Himalaya	16.6	42.1	−5.6	
		Time Step 40–47 Ma, 2 Blocks		
India	−23.34	−176.36	25.3	*Patriat and Achache* [1984]
Frontal triangle	39.2	4.6	−5.4	

northeastward decreasing offset of the Altyn Tagh fault [*Van Der Woerd*, 1998] along the Tarim (∼150 km north of the Qiangtang block, ∼130 north of the Qaidam block, ∼105 km north of the Qilian Shan block), and the correspondingly decreasing slip rates (30, 25, and 21 mm/yr). This is one of the main areas of discrepancy between GPS and Holocene rates, which we interpret to be due to transient, decennial or centennial strain [*Bendick et al.*, 2000; *Shen et al.*, 2001; *Meriaux et al.*, 2000]. The width of the gap along the Qilian Shan (∼100 km) corresponds to the shortening absorbed across the Qilian and other thrusts to the south (Qaidam, Qiman Tagh), consistent with the evidence summarized by *Meyer et al.* [1998]. There is also an eastward decrease in shortening along the Qilian Shan, compatible with the topographic gradient observed [*Meyer et al.*, 1998].

[32] If, as we chose to illustrate in this time step, the forward component of motion of Tibetan blocks toward the east (Figure 3b) were transmitted to south China, with negligible shortening in the Longmen Shan, as indicated by early GPS campaigns (<5 mm/yr) [*King et al.*, 1997], south China would move back west-northwest, by ∼90 km near Shanghai, which would be 30% more than predicted by extrapolating back the present-day rate (∼12 mm/yr) derived from VLBI measurements [*Heki*, 1996]. Sinistral motion along the Haiyuan and Qinling-Dabie faults would generate fairly large amounts of extension around the Ordos block (∼30 km in the Yingchuan graben to the west of the block, and ∼30 km in the Fen He graben to the east), as well as in the north China plains (∼30 km). There would be an eastward decreasing, stepwise, gradient of slip from the Haiyuan to the Qinling and then to the Dabie Shan faults, consistent with successive loss of motion into the three rift zones. Although qualitatively compatible with the deformation styles observed across north China, all the finite amounts of displacements computed are too large by about 30%. This suggests to us that the shortening rate in the Longmen Shan has been at least ∼5 mm/yr in the last 5 Myr. Recent GPS data in SE Tibet [*Wang et al.*, 2001], contrasting with previous ones [*King et al.*, 1997; *Chen et al.*, 2000], or with geological results [*Burchfiel et al.*, 1996], are compatible with 5 to 11 mm/yr of shortening in and west of the Longmen Shan. This would resolve the inconsistency above and might be in keeping with the 1 cm/yr of shortening rate inferred across the range by *Avouac and Tapponnier* [1993] and *Peltzer and Saucier* [1996].

[33] In the southeastern part of the collision zone, the dextral Sagaing fault accommodates the large southward back motion between India and Indochina, at an average slip rate of 33 mm/yr. Spreading in the central Andaman Sea, at the southern end of the fault, absorbs 165 km of motion. To the south, about two thirds of this movement must be transmitted to the Nicobar fault (24 mm/yr), a structure whose importance has been thus far overlooked. This is required to obtain compatible finite motions. Without this fault, the southward movement of the Myanmar block, dragged back by India, would drive the southern part of Sumatra southward. The island would thus be dismembered by a gap whose width would imply shortening of Himalayan proportions (∼2 cm/yr) along the Barisan Mountains. This is clearly not observed. Only about one third of the motion on the Sagaing fault is transmitted to the Barisan or Great Sumatran Fault (10 mm/yr, consistent with the average rate obtained between 2 Ma and the present by *Sieh and Natawidjaja* [2000]. The gap between the Myanmar block and the Bengal delta region corresponds to subduction of the Indian plate beneath the folded accretionary wedge of Arakan Yoma [e.g., *Le Dain et al.*, 1984].

[34] Looking forward in time (Figure 3b), the torque exerted by the northward motion of Myanmar and India to the west, and the east-southeastward motion of Tibet and south China to the north and east, drives Indochina to spin clockwise on itself, while keeping a relatively stable latitudinal position. While south China also rotates clockwise (Figure 3b), it does so faster along its Red River boundary with Indochina, which results in ∼4 mm/yr of dextral slip there [*Replumaz et al.*, 2001]. Northwest of India, the gap north of the Pamirs corresponds to ∼95 km of north-south shortening at a rate of ∼2 cm/yr [*Liu*, 1993; *Burtman et al.*, 1996], similar to that in the Himalaya.

[35] The west Tibet block and west Kunlun sliver push the western part of the Tarim northward, inducing its forward clockwise rotation (Figure 3b). As this rigid block rotates, westward increasing shortening is absorbed north of it, within the Tian Shan [*Avouac et al.*, 1993]. On Figure 3a, this corresponds to the simplified gap visible south of the range, whose width decreases from the southwest (100 km) to the northeast (50 km), consistent with an eastward decrease in shortening rate from ∼2 cm/yr [*Abdrakhmatov et al.*, 1996] to ∼1 cm/yr. Recall that deformation north of this gap is not modeled here.

[36] By far the greatest incompatibility of the 5 Ma-0 retrodeformation step occurs in western Tibet, along the curved, conjugate strike-slip boundaries of the Qiangtang block (Figures 2c and 1a). This implies that this block was

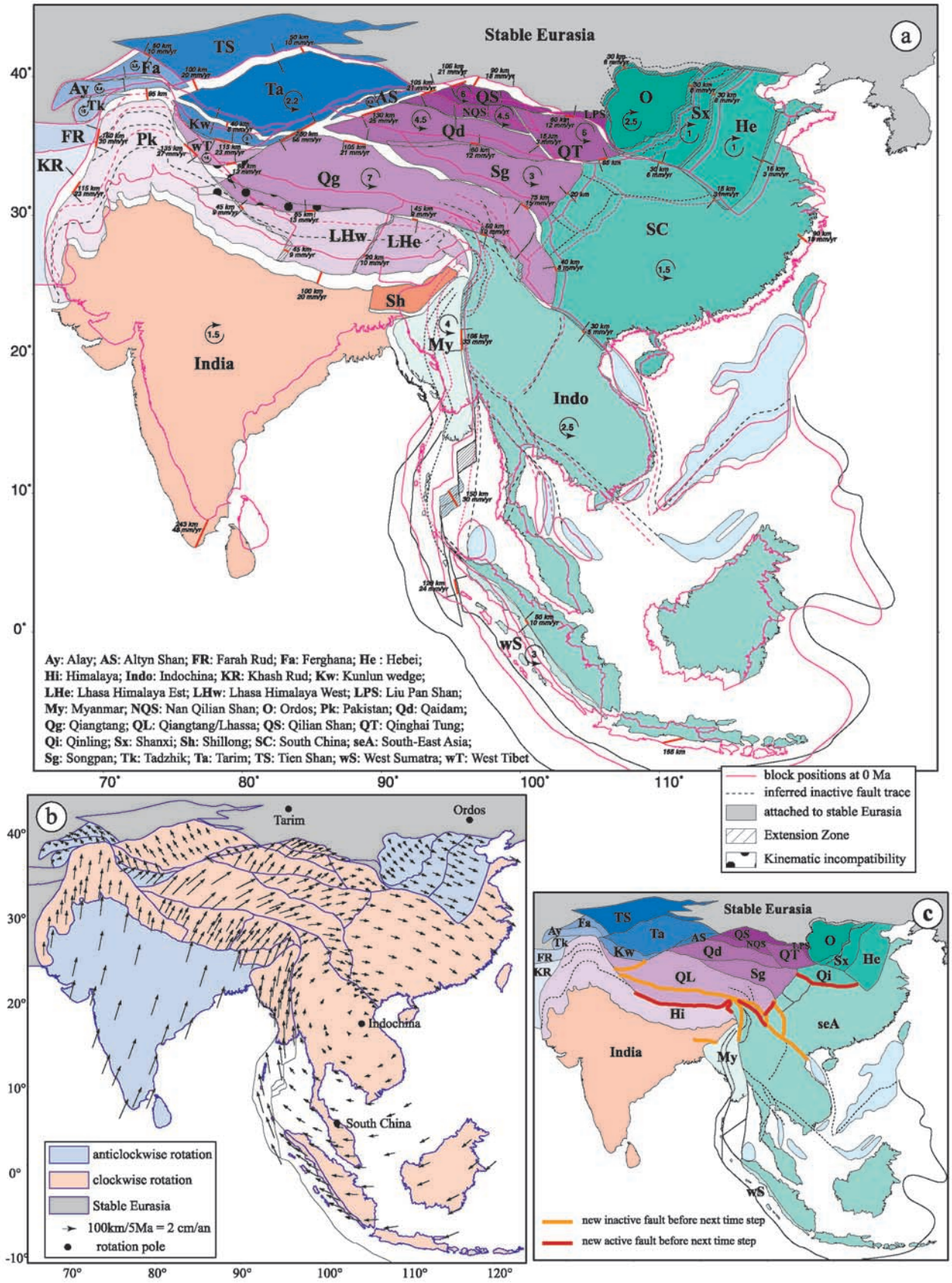


Figure 3. Time step reconstruction 0–5 Ma. (a) Deformation from block motion. (b) Displacement field. (c) New block positions and contours at 5 Ma.

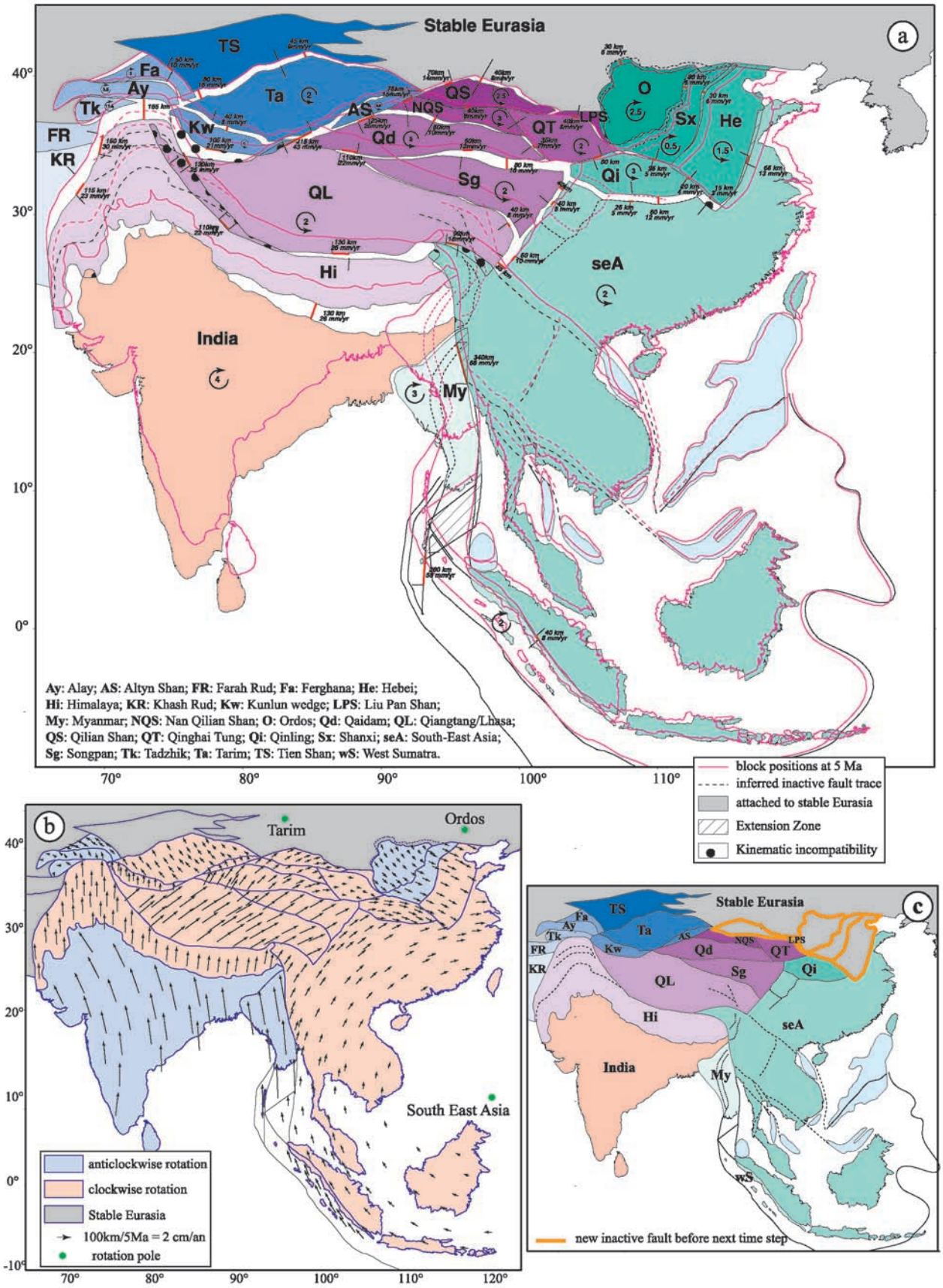


Figure 4. Time step reconstruction 5–10 Ma. (a) Deformation from block motion. (b) Displacement field. (c) New block positions and contours at 10 Ma.

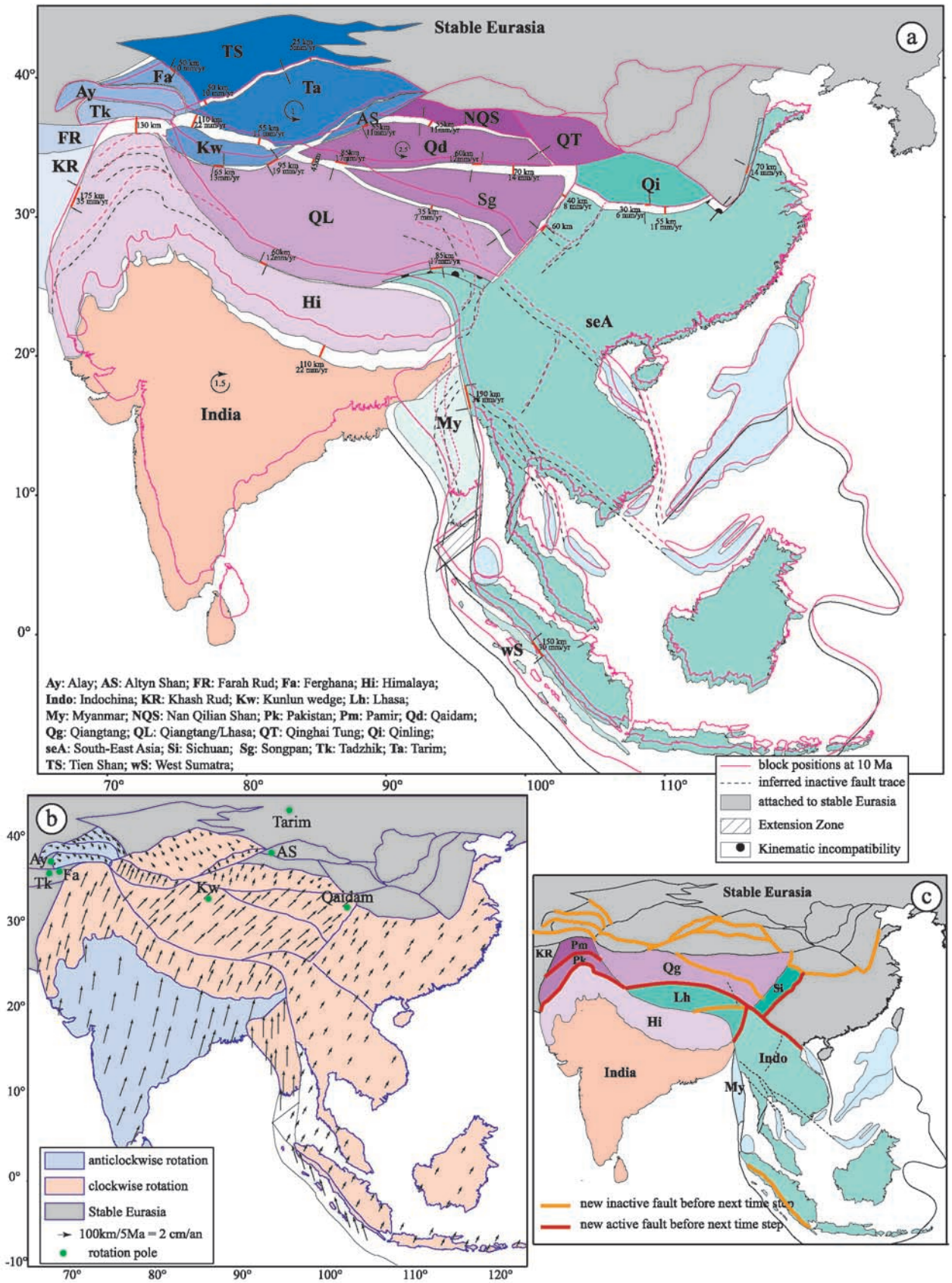


Figure 5. Time step reconstruction 10–15 Ma. (a) Deformation from block motion. (b) Displacement field. (c) New block positions and contours at 15 Ma.

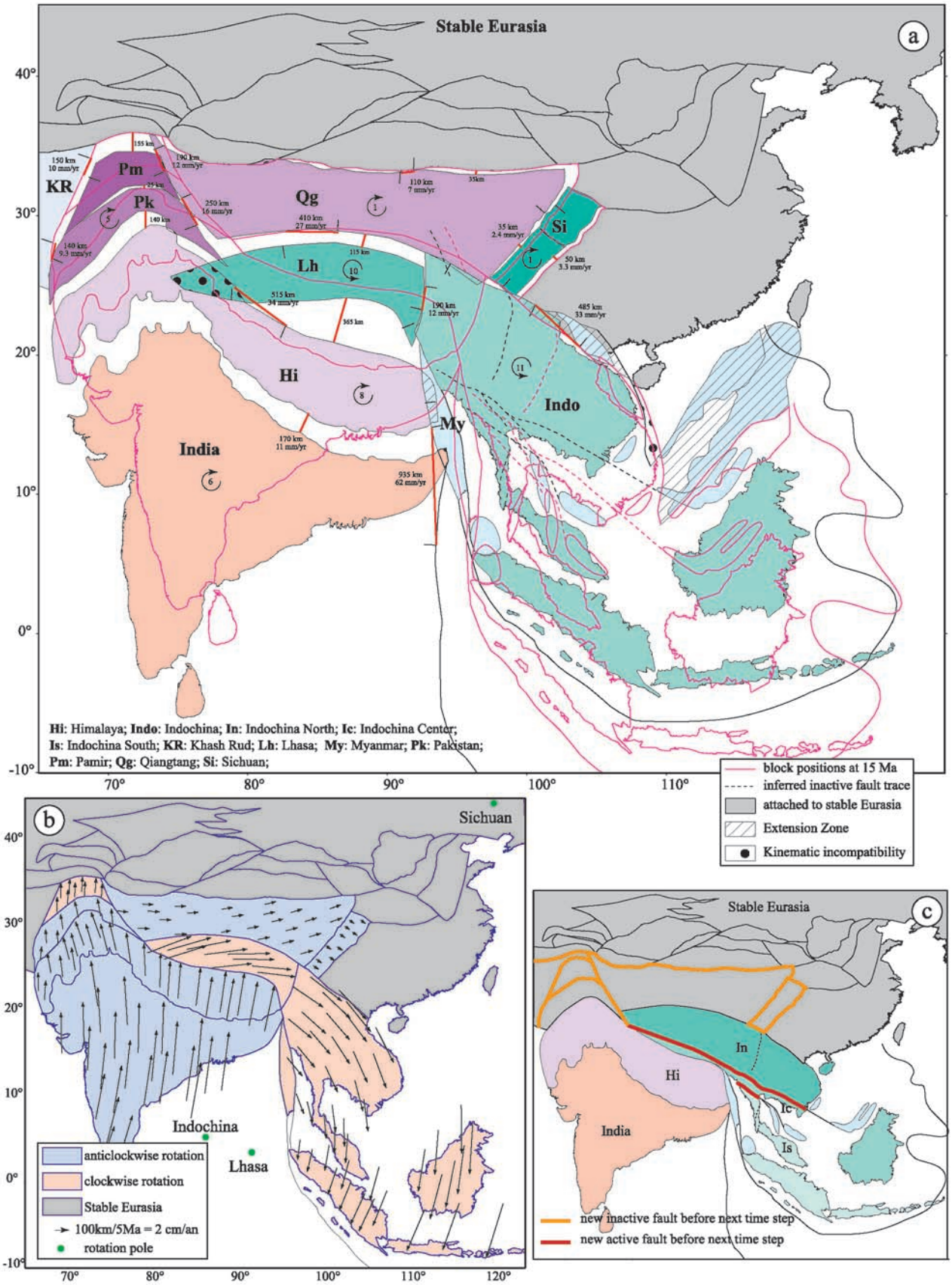


Figure 6. Time step reconstruction 15–30 Ma. (a) Deformation from block motion. (b) Displacement field. (c) New block positions and contours at 30 Ma.

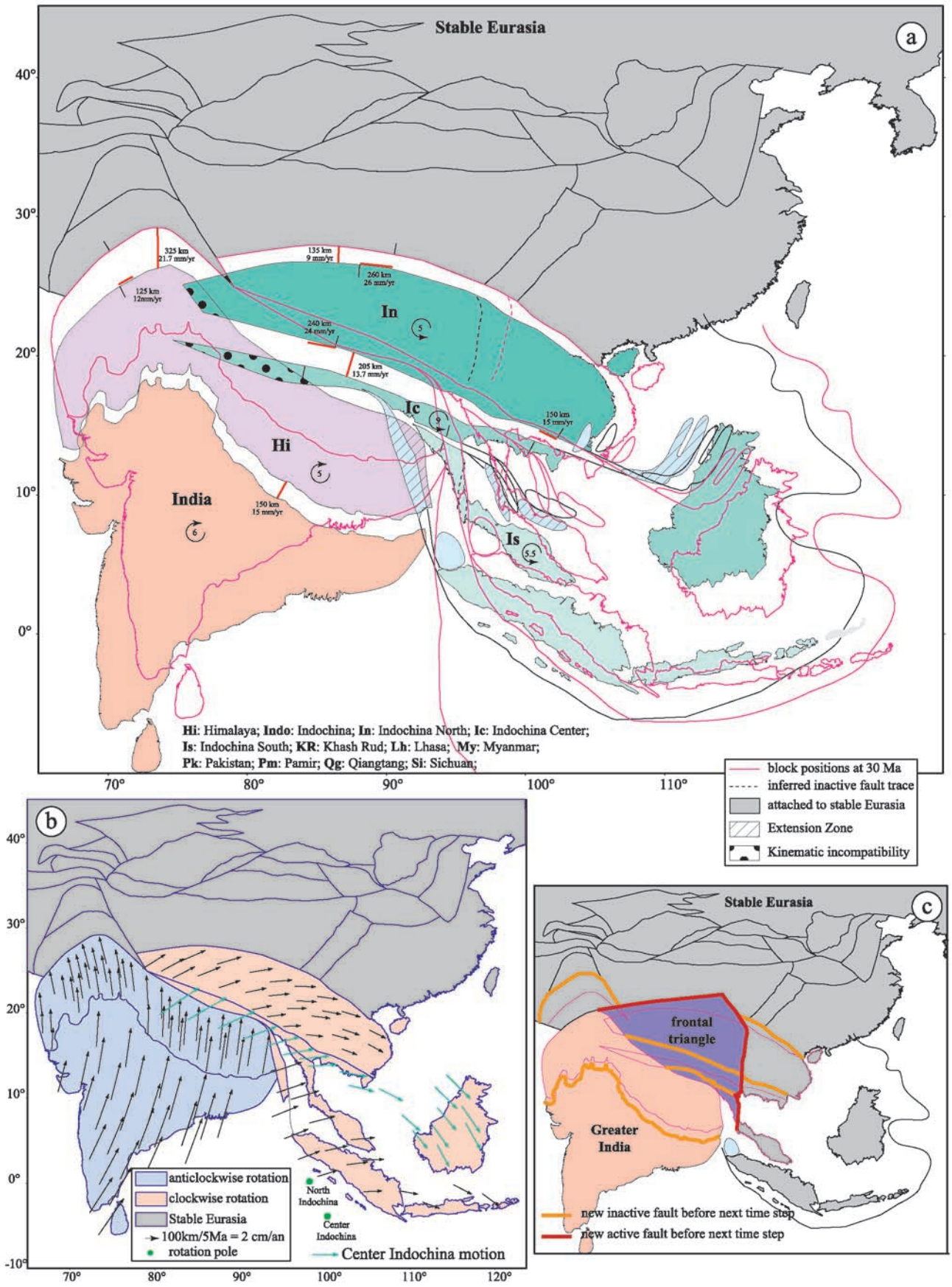


Figure 7. Time step reconstruction 30–40 Ma. (a) Deformation from block motion. (b) Displacement field. (c) New block positions and contours at 40 Ma.

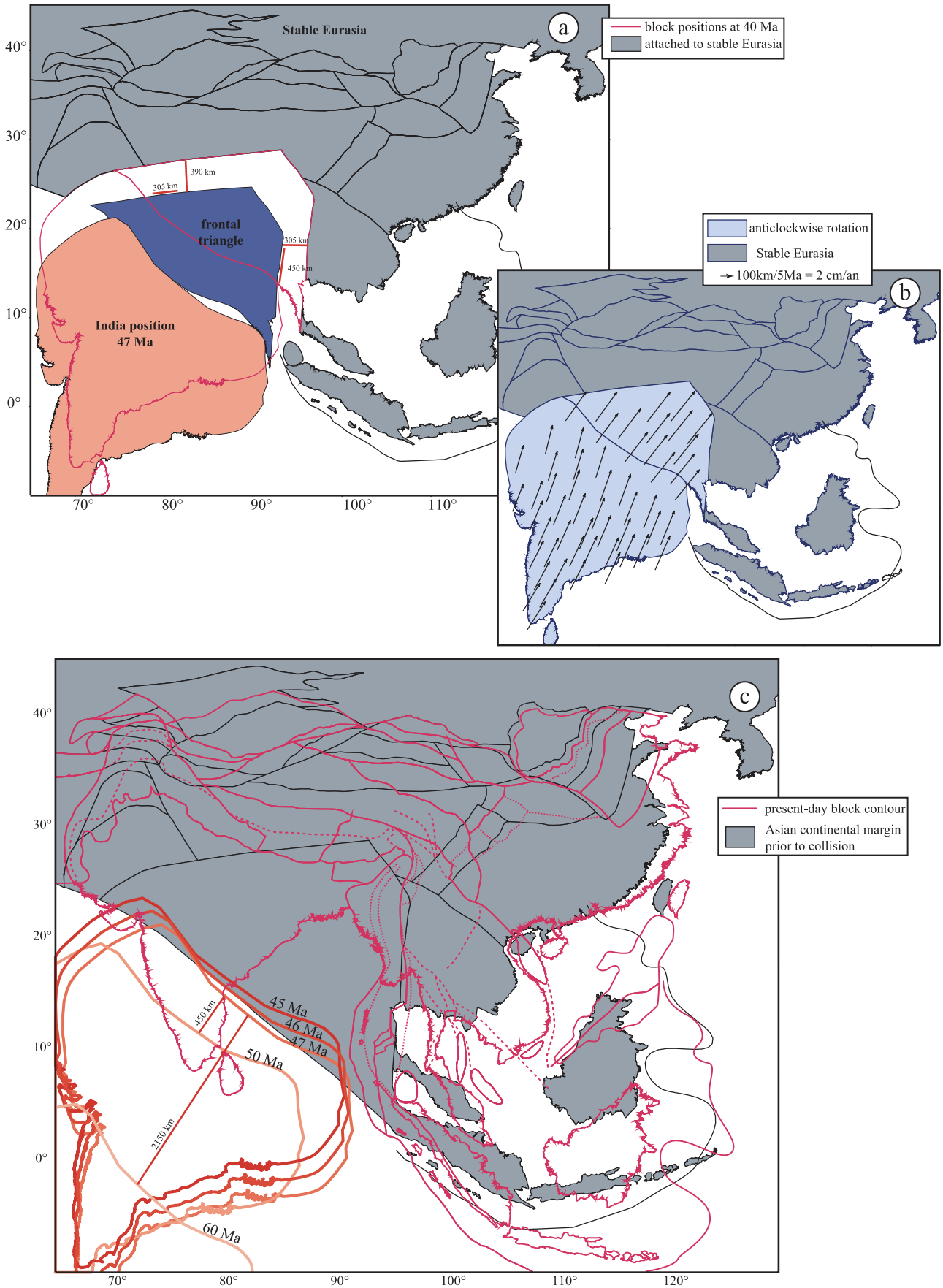


Figure 8. Time step reconstruction 40 Ma to collision onset. (a) Deformation from block motion. (b) Displacement field. (c) Asian continental margin and India positions prior to collision.

deformed and bent, loosing its torsional rigidity. Significant amounts of southward increasing east-west extension within Qiangtang [*Armijo et al.*, 1989; *Yin et al.*, 1999] and Plio-Quaternary folding north of the Karakorum fault [*Matte et al.*, 1997] would be required to alleviate this incompatibility. The gap along the Qiman Tagh, where active shortening appears to be less than in the Qilian Shan, would thus be also reduced.

[37] Figure 3c shows the fault pattern activated prior to 5 Ma, after restoration of the block contour continuity. At ~5 Ma, the Red River fault apparently ceases to be dextral, coevally with the onset of normal faulting and rapid exhumation in the Diancang Shan [*Leloup et al.*, 1993], and with the beginning of thrust inversion in the basins of the Gulf of Tonkin [*Replumaz et al.*, 2001]. Since the finite amount of slip on the eastern strands (Kyaring Co, Beng Co) of the Karakorum-Jiali fault zone appears to be small, ~20 km [*Armijo et al.*, 1989], we infer that it was not active prior to 5 Ma either. The Xiaojiang fault also appears to have a small finite offset [*Wang et al.*, 1998] and may have been in existence for at most ~5 Myr. Consequently, we assume that prior to ~5 Ma Southeast Asia temporarily formed a single large block, with Indochina and south China rigidly welded together. The pre-5 Ma boundaries within Southern Tibet also become simpler. The active Yarlung-Zangbo suture was probably simply connected with the dextral Karakorum fault, separating a ''new'', wholesale Pamir-Himalaya block from a larger Qiangtang-Lhasa block. The topographic limit of eastern Tibet was probably a large thrust (Litang-Longmen Shan thrust) absorbing a significant fraction of the eastward component of motion of the Qiangtang and Kunlun blocks relative to south China. Prominent east-west folding of the Mesozoic cover of the Yangzi platform in the southern Qinling Shan, north of the Sichuan Basin, leads us to introduce a new boundary south of and parallel to the Qinling fault, the South Qinling thrust (Figure 3c).

3.2. Time Step 5–10 Ma

[38] The new positions of the new blocks defined above, after backward rotation on the sphere at 10 Ma, are shown on Figure 4a. Although the overall displacement field in this second step is similar to that in the first, there are some significant differences.

[39] The position of India is now derived from ocean floor magnetic anomalies according to the reconstruction of *Patriat and Achache* [1984], which does not overlap in time with that of NUVEL-1A [*DeMets et al.*, 1994]. This induces a sharp, artificial discontinuity in India's motion. Although the average north-south component of motion is about the same (250 km, corresponding to ~5 cm/yr), a large, additional backward clockwise rotation (4° between 10 Ma and 5 Ma, instead of 1.5° between 5 Ma and 0) is introduced. This rotation, due to mismatch between the two approaches, induces in turn several artifacts. The most striking difference is that the mean slip rate along the Sagaing fault jumps from 33 mm/yr, probably a lower bound between 5 Ma and the present, to 68 mm/yr between 5 and 10 Ma, a value greater than plausible. The Southeast Asian megablock has become large enough that, through lever arm amplification, small displacements on one boundary can yield unacceptably large ones on another. The motion of this block is essentially constrained by the slip rates along the Sagaing and the South Qinling faults. A slip rate of 68 mm/yr on the Sagaing fault, which is likely much too fast, would yield 60 km of shortening between north and south China (12 mm/yr on the South Qinling fault), which is certainly also an upper bound. This is a direct consequence of the exaggerated rotation of India, which induces too much convergence along the northeastern boundary of the Southeast Asian block.

[40] Slip partitioning now occurs in a simpler manner in the southern part of Tibet, with the dextral Karakorum-Yarlung-Zangbo fault being almost parallel to the Himalayan thrust. The forward translation of Tibet toward the east (Figure 4b) is ~130 km (at a rate of 26 mm/yr). Although the gap along the Himalaya increases westward, which is most likely another artifact due to the exaggerated rotation of India, the average shortening along the range is on order of 130 km (an upper bound).

[41] In northern Tibet, shortening migrates back southward, and occurs mostly along the edges of the Qaidam block. The amounts are ~40 km in the Qilian Shan, 50 km in the Nan Qilian Shan, and 80 km north of the eastern part of the Kunlun fault, all of them upper bounds. Such shortening is absorbed by several parallel thrusts, distributed within the Qilian, Nan Qilian, Burhan Budai and Songpan ranges. During this earlier stage, the strike-slip rate along the Kunlun fault is constant at 12 mm/yr, but along the Haiyuan fault, it is smaller (8 mm/yr). There is still a gradient of slip rate along the Altyn Tagh fault, from 43 mm/yr in the south to 25 mm/yr in the north (again upper bounds). The eastward component of motion of the central Tibetan blocks relative to south China (Figure 4b) are absorbed by shortening in the Longmen Shan and on the Litang thrust. They amount to ~85 km in the south, between south China and the Qiangtang-Lhasa block, and ~40 km in the north between the Songpan and South China blocks.

[42] The displacement fields in the western and northeastern parts of the collision zone are similar to those in stage 1 (Figure 4b). The main changes in the active fault pattern prior to 10 Ma concern the northeastern part of the collision zone (Figure 4c). Given a total displacement on the Haiyuan fault on the order of 100 km (95 ± 15 km [*Gaudemer et al.*, 1995] and ~125 km [*Lasserre*, 2000]), the fault comes into existence in our reconstruction at about 10 Ma. Motion on this fault being intimately linked with block rotation and rifting in north China [*Peltzer et al.*, 1985; *Gaudemer et al.*, 1995] and with shortening in the northern Qilian Shan [*Meyer et al.*, 1998], the corresponding block boundaries shut off prior to ~10 Ma, coevally with that fault. Thus these blocks, including the Ordos and the northern Qilian Shan sliver, become kinematically welded to stable Asia at that time.

3.3. Time Step 10–15 Ma

[43] Figure 5 shows the third reconstruction stage. With regard to the motion of India relative to Siberia, there is no change at 10 Myr, thus no mismatch or incoherence. India moves back southward by ~250 km, while rotating counterclockwise (1.5°) as in the first stage. The corresponding slip rate along the Sagaing fault is 38 mm/yr. The directions of Asian block motions, however, change in a significant manner.

[44] The northeastward motion of the Songpan block (Figure 5a) generates 60 km of strike-slip and 70 km of strike-perpendicular shortening along the Kunlun fault. The shortening component is absorbed by underthrusting beneath the Burhan Budai range and north of the Kunlun fault trace. Shortening between the Qiangtang and Songpan blocks along the Xianshui He fault is absorbed in a coherent way within the Songpan block, along several parallel thrusts.

[45] The wide gap between the Tarim and the Kunlun wedge represents the amount of Tarim basement subducted beneath this wedge along the western Pamir range front. Continental subduction there increases westward (110 km to the west, 55 km to the east), and is oblique, leading to 70 km of sinistral slip along the Karakax fault (at ~13 mm/yr), south of the West Kunlun range, a result of slip partitioning. Nearly pure, downdip subduction of the Tadjik block basement, on the other hand, occurs beneath the north rim of the Pamirs (at 23 mm/yr), corresponding to the 130-km-wide gap there. There is still significant, though smaller, shortening in the Tian Shan and Chatkal ranges (~50 km, 1 cm/yr in the west), linked by dextral shear transfer along the Talas Ferghana fault (~1 cm/yr). Finally, nearly pure sinistral slip occurs along the Darwaz-Quetta fault (~175 km) at a rate of 35 mm/yr.

[46] Major changes in the active fault pattern occur around 15 Ma (Figure 5c). This is the time when sinistral motion along the Red River fault, opposite to its present-day sense of slip, stops [*Leloup et al.*, 1995]. Although the westward continuation of the Red River-Ailao Shan shear zone has not yet been accurately mapped, it likely extended along the southern edge of the Markham basin [*Leloup et al.*, 1995; *Roger et al.*, 2000], then possibly along the Bangong suture (dashed line in Qiangtang block on Figure 1) to meet westward with the Karakorum fault near Bengong lake [*Tapponnier et al.*, 2001]. Cooling $^{39}Ar/^{40}Ar$ ages (~17 Ma), in dextrally sheared gneisses along the Nujiang valley, indicate that the Gaoligong fault, separating the Lhasa block from Indochina (Figure 5c) was active prior to 15 Ma, and perhaps as early as 25 Ma [*Zhong and Ding*, 1991].

[47] With the bulk of sedimentary deposition in the Qaidam basin occurring after ~5 Ma [*Meyer et al.*, 1998; *Métivier et al.*, 1999], and most of the calc-alkaline volcanism south of the Kunlun fault postdating ~15 Ma, subduction and regional shortening north of the Kunlun probably did not start much before this date. Similarly, extrapolation of shortening rates in the Tian Shan and of the Tarim block's rotation rate implies that deformation was less north of the Tarim prior to 15 Ma. Decreasing sedimentation rates in the Tarim and Junggar basins [*Métivier et al.*, 1999], as well as plausible finite amounts of Tertiary shortening across the Tian Shan [*Avouac et al.*, 1993] corroborate the idea that crustal thickening along the range started in the mid Miocene.

[48] We therefore assume that, prior to 15 Ma, central Asian blocks north of the Pamir and Kunlun fault were essentially attached to Siberia. This implies that the Altyn Tagh fault east of its Karakax segment had accrued most of its finite offset (~460 km), consistent with field observations. Note also that the Karakax fault at 15 Ma had become continuous with the Kunlun fault, as implied by the great similarities of rock assemblages along both faults.

[49] Motion along the Sagaing fault, corresponding to a total displacement of ~700 km, had by then led to closure of the Andaman Sea basin. This suggests that its southernmost stretch was not active prior to 15 Ma. Previously, the transtensive, still dextral boundary between India and Indochina was probably more diffuse, with en echelon pull-apart basins, now hidden beneath the thick deposits of the Burmese lowlands [e.g., *Peltzer and Tapponnier*, 1988; *Le Dain et al.*, 1984]. At this stage, we integrate the now unfolded Indo-Burman sediments to the oceanic Indian plate. Only a narrow sliver of basement, deprived of the accreted Arakan Yoma prism, thus subsists as the Myanmar block.

3.4. Time Step 15–30 Ma

[50] Figure 6a shows the results of backward deformation at 30 Myr. This fourth stage covers a 15 Myr period, three times longer than the previous ones. It is primarily constrained by the motion of Indochina deduced from south China seafloor magnetic anomalies [*Briais et al.*, 1993]. This motion corresponds to back slip restoration of ~485 km of sinistral displacement along the Red River fault, at a rate of ~33 mm/yr, with transpression in the west and transtension in the east. The eastward increasing transtensive component progressively exhumed the Ailao Shan gneisses [*Leloup et al.*, 1995; *Harrison et al.*, 1996]. The hatched area on Figure 6a corresponds to the width of Oligo-Miocene seafloor in the northeast part of the South China Sea but encroaches on a zone of diffuse continental stretching in the southwest [*Briais et al.*, 1993].

[51] The Lhasa block moves back westward, like Indochina, while rotating back counterclockwise by 10°. It also slides back southward ~190 km along the Gaoligong fault. Motion on this fault at ~12 mm/yr reduces what would otherwise become a large overlap misfit zone between the Qiangtang and Lhasa blocks (to the west) incompatible with the shortening observed at this time in western Tibet. A significant overlap remains, however, between the western tip of the Lhasa block and the Himalayan block, which requires that this tip be bent and squeezed between the Red River-Bangong and Yarlung-Zangbo boundaries, losing rigidity during this period. In fact, this is a period during which particularly large deformations occur in central Tibet, in tune with crustal thickening of this part of the plateau. As much as 115 km of coherent oblique shortening, probably distributed on thrusts north of the Bangong suture (simplified gap along this suture on Figure 6a), takes place between the Lhasa and Qiangtang blocks. The amount of left-lateral motion between the blocks reaches 410 km (27 mm/yr). Concurrently, between the Lhasa and Himalaya blocks, the amount of dextral shear and of oblique shortening along the Karakorum-Zangbo boundary reach 515 km (34 mm/yr), and a maximum of ~380 km, respectively. This shortening is so unevenly distributed from east to west that strong bending of the Lhasa block is required, bringing the average shortening rate north of the Zangbo suture to ~13 mm/yr. Our knowledge of the geology of tectonic boundaries within south central and western Tibet at that time is so poor that it is difficult to decide whether the rigidity assumption fails altogether or whether motion on only a few faults separating smaller blocks might help solve the deformation compatibility problems encountered.

[52] The average shortening rate along the Himalaya, probably mostly on the Main Central Thrust, is only 11 mm/yr (170 km), a consequence of dominant extrusion during this time step. Although total forward movement of Qiangtang along the Kunlun-Karakax fault is relatively small (115 km), it continues at ~7 mm/yr, while the fault propagates eastward. Part of this motion toward the east (Figure 6b) is absorbed in the Longmen Shan (35 km), and in the roughly NNE-SSW fold zone that bounds the Sichuan basin to the east (50 km).

[53] Around 30 Ma, the active fault pattern changes markedly again (Figure 6c). The northern boundary of the paleo-Tibetan highlands appears to shift south of the Jinsha suture, near a belt marked by Eocene (50–40 Myr) intrusive, calc-alkaline granitoids [*Roger et al.*, 2000]. Thus, prior to 30 Ma, we assume that the Red River fault roughly follows the northernmost limit of large-scale deformation in Asia. The Kunlun fault is not active anymore. The dextral boundary between the Himalaya and Lhasa block has not yet propagated along the Karakorum fault. Prior to 30 Ma, the middle part of the Indochina block was being sliced by the sinistral 3 Pagodas and Wang Chao faults, whose strike-slip displacements clearly predate 30 Ma [*Lacassin et al.*, 1997]. Although the westward continuation of these faults in South Tibet is unknown, it is likely that at least one of them extended past the west Himalayan syntaxis not far north of the Zangbo suture. One possibility would be that the Nyainqengthangla shear zone [*Tapponnier et al.*, 1986; *Armijo et al.*, 1989] was once continuous with the Wang Chao fault. To the east this fault may have reached the Sarawak extensional basin along the northwestern coast of Borneo. The 3 Pagodas fault probably terminated in the extensional basins of the Thailand Gulf.

3.5. Time Step 30–40 Ma

[54] The reconstruction becomes quite schematic at this stage, given the dearth of quantitative data. The slicing of Indochina by the Wang Chao and 3 Pagodas faults corresponds to another, earlier phase of extrusion (Figure 7a). Final backward motion along the Red River fault (up to 260 km, 26 mm/yr) closes the Yinggehai basin and the Leizhu rift in the Gulf of Tonkin as well as rifts between Hainan and Macclesfield Bank [*Briais et al.*, 1993]. Motion along the Wang Chao fault closes the Sarawak basin (up to 240 km, 24 mm/yr). Motion along the 3 Pagodas fault closes the Gulf of Thailand (up to 100 km, 10 mm/yr). Such motions induce large incompatibilities in southwest Tibet, and might imply about 400 km of additional dextral movement along the Zangbo boundary. Such extrusion is coupled with the thickening of the Lhasa-Indochina block accounting for the late Eocene rise of the Southern Tibet plateau. Like Qiangtang in later stages, this block probably lost its rigidity while being shortened and squeezed out eastward.

[55] Going back further in time amounts to entering a realm of almost unconstrained speculation. Nevertheless, before 40 Ma (Figure 6c), the deformation pattern may have been simpler, with most of the strain localized along the boundaries of a roughly triangular zone north of India, and with much less asymmetry, as suggested by plasticine indentation experiments [*Peltzer and Tapponnier*, 1988]. The western limit of this "frontal triangle" might have been close to the Bangong suture. Its eastern boundary would have been located along a fault zone composed of the Ranong fault across the Malay Peninsula in the south, of the Uttaradit-Dien Bien Phu fault in Vietnam, and of the Benzilan-Jinsha fault in Yunnan and Sichuan.

3.6. Time Step 40–50 Ma

[56] For this step (Figure 8a), the only constraints left are the position of India [*Patriat and Achache*, 1984], and the existence of intrusive Eocene granites in the Tanggula range along central Tibet's Bangong suture [*Roger et al.*, 2000], which implies mountain building and perhaps lithospheric mantle subduction there [*Tapponnier et al.*, 2001]. Structures within the frontal triangle are poorly known, but we assume that deformation was localized along the boundaries of this triangle. Oblique conjugate shortening (dextral in the east, sinistral in the west) thus probably took place. The amounts of shortening could have been large, with 300 to 400 km of strike-parallel slip and strike-perpendicular shortening inducing crustal thickening in the innermost core of the early Eocene Tibet. In the east, dextral slip along the Ranong fault could have led to the opening of the Eocene Mergui basin [*Tapponnier et al.*, 1986], a poorly explained feature of the southeastern Andaman basin.

[57] Given the restored position of the southern margin of Tibet deduced from our five stages backward reconstruction, the onset of the deformation of Asia due to collision would have occurred around 50 Ma. Although this age clearly depends on the cascade of choices and inferences we made (e.g., total shortening in the Himalaya, position of India from *Patriat and Achache* [1984], etc.), any earlier onset (e.g., ~55 Ma) would require significant shortening in Mongolia and Sayan, and/or increasing amounts of continental subduction of an increasingly greater India (Figure 8c).

4. Overall Displacement Field

[58] The displacement field, relative to stable Eurasia, determined using the Euler poles derived in our reconstruction for each time step, must be compared with other studies, and with additional data sets not used as input.

[59] For the first step (0–5 Ma), the overall motion of Tibetan and eastern Asian blocks has a large eastward component, which decreases eastward, consistent with present-day extrusion (Figure 3b). The largest discontinuities in the directions of displacement vectors are along the Altyn Tagh-Karakax, Karakorum, Kunlun and Haiyuan faults and the largest discontinuities in amplitude are along the Himalayan front and along the Altyn Tagh, western Kunlun, and Sagaing faults. Indochina rotates around a pole located in North Vietnam. This block, which encompasses all of Southeast Asia at this stage, is, in fact, dragged northward on its west side by the Myanmar block, which follows the northward motion of India, and eastward on its northeast side by south China, which is pushed by Tibet along the Longmen Shan. Such a rotation is compatible both with dextral motion along the Sagaing fault and dextral-extensional motion along the Red River fault.

[60] This 0–5 Ma displacement field, based mainly on Holocene average slip rates, shows similarities and significant differences with that derived from the most recent and broad-based GPS results [*Wang et al.*, 2001]. To a first

order, within the fairly large uncertainties that remain in either approach, the agreement between the directions of movements in the Himalaya, Tibet and eastern China is quite good. In terms of the magnitudes of the movements, however, the GPS shows in general smaller motions. One chief reason for this appears to be that the decadal boundary motion of India in the Eurasian reference frame is as much as 20% slower than the long-term displacement rate consistent with NUVEL-1 (37 versus 47 mm/yr [*Wang et al.*, 2001]). The particularly large motions we obtain in western Qiangtang are an unrealistic consequence of our modeling this entire block as "rigid", which leads to obvious incompatibilities. Unfortunately, they cannot be compared against GPS results for lack of data there. The rotation we obtain for the Tarim is significantly different from that consistent with GPS data [*Abdrakhmatov et al.*, 1996; *Shen et al.*, 2001; *Wang et al.*, 2001], which may imply that Avouac and Tapponnier's long-term pole relative to Siberia is different from the present pole. Note however that the density of GPS stations and number of survey epochs is still insufficient in most places to assess whether deformation is distributed or to define blocks that rotate. The swing in the directions of movements around the eastern Himalayan syntaxis is more pronounced in the GPS data [*King et al.*, 1997; *Chen et al.*, 2000; *Wang et al.*, 2001] than in our reconstruction. This discrepancy surely stems in large part from the fact that both of the syntaxes are the main places where the rigidity assumption fails in most stages of our reconstruction. Nevertheless, in terms of displacement magnitudes, the discrepancy is small. In particular, both approaches show a marked decrease in SE motion (5–10 mm/yr [*Wang et al.*, 2001]) across the Longmen Shan and Xiao Jiang fault, consistent with previous modeling [e.g., *Avouac and Tapponnier*, 1993; *Peltzer and Saucier*, 1996]. They also show a pronounced discontinuity across the Red River Fault, consistent with oblique, extensional-dextral motion along it. This latter boundary remains the most problematic in all kinematic models of the collision zone, with large discrepancies in both observed or predicted directions and amounts of motions. South of the Red River, our reconstruction shows relatively small (<5 mm/yr) NE directed movements, while the GPS results in the same reference frame show south to SW directed movements of similar magnitudes. The GPS results of GEODYSSEA indicate beyond ambiguity that most of Indochina, including the Sunda shelf, behaves as a rigid block but lead to large (~3 cm/yr) roughly EW movements in the same area [*Wilson et al.*, 1998; *Walpersdorf et al.*, 1998; *Chamot-Rooke and Le Pichon*, 1999; *Michel et al.*, 2000]. Such discrepancies are likely largely due to the fact that the northern tip of Indochina deforms and is not rigidly attached to the Indochina plate. Current motions on several faults, among which the Nanting and Wanding faults [*Lacassin et al.*, 1997] in the Golden Triangle region of Burma and China, and the Dienbienphu fault in Vietnam, still poorly studied in the field, probably take up part of the strong regional bending resulting from the local indentation of India's eastern corner into the region where Indochina, China and Tibet meet. In summary, though disagreements, centered around fault slip rates, remain between GPS and geologic results, they differ from region to region. Acceptable matches are obtained for the Main Frontal Thrust [e.g., *Bilham et al.*, 1997] and the Kunlun fault [*Van der Woerd et al.*, 2000], as found also for the North Anatolian fault [*McClusky et al.*, 2000], but large differences exist most prominently along the Altyn Tagh fault. This major disagreement is now under scrutiny [e.g., *Wang et al.*, 2001; *Mériaux*, 2002]. Geological cosmogenic ages may be biased by some unknown source of error, but it is also clear that, for the moment, in Tibet, the GPS array is hardly dense enough to allow precise determinations of most fault slip rates.

[61] Starting with the second time step, between 5 and 10 Ma, comparison with GPS is of course meaningless. This stage is a transitional one, with blocks moving mostly northward in the southern and eastern parts of the collision zone, and significantly eastward in the central and northern parts (Figure 4b). While slivers and blocks northeast of Tibet are strongly pushed eastward, south China is not. Locking of the Red River fault prevents eastward motion of south China during that period. It is instead welded with Indochina into a Southeast Asian megablock whose wholesale rotation resembles that of Indochina in the previous stage, but with a pole located farther east, between Borneo and Taiwan. The resulting movement is mostly north to northeastward. As for Indochina between 5 Ma and the present, the motion of this block was driven principally by the torque imparted along the Sagaing fault by India's northward drift. Large incompatibilities continue to characterize deformations near either of the Himalayan syntaxes.

[62] Between 10 and 15 Ma, most of the blocks move dominantly northward with the exception of Qiangtang and Songpan on one hand, and Tarim and Ferghana on the other (Figure 5b). This epoch thus corresponds to a lull in extrusion, while thickening is the predominant process. The most significant incompatibility persists near the eastern syntaxis.

[63] In contrast with the 10–15 Ma stage, between 15 and 40 Ma, Tibetan and Southeast Asian blocks move again dominantly eastward and southeastward, and wholesale lateral extrusion appears to absorb most of the convergence (Figures 6b and 7b). This epoch corresponds to the periods during which Indochina escapes along the Red River fault, and southern slivers of it, along the Wang Chao and 3 Pagodas faults. The largest discontinuities in the directions of displacement vectors are along the Red River, Karakorum-Zangbo, Shan-Sagaing and Kunlun faults.

[64] Albeit speculative, the first stage of deformation (Figure 8b), corresponding to our last time step, between 40 and ~47 Ma, shows dominant northward motion, with mostly oblique, conjugate crustal thickening, and no extrusion. The underlying kinematic and mechanical inference is that the remarkable asymmetry that characterizes tectonic styles and motions within the collision realm at latter epochs has not yet developed. Overall, the displacement field maps (Figures 3b to 8b) thus illustrate clearly the oscillations between the 2 main processes of continental deformation, lithospheric block extrusion and crustal thickening coupled with mantle subduction [*Meyer et al.*, 1998; *Peltzer and Tapponnier*, 1988].

[65] The main tenet of the model (deformation localized along faults) is of course manifest on the maps, where each large slipping fault is reflected by a discontinuity in trend and/or amplitude of the displacement vectors. Only across small, numerous discontinuities might the displacement

Table 3. Quantification of the Continental Deformation

Deformation Type	0–5 Ma	5–10 Ma	10–15 Ma	15–30 Ma	30–40 Ma	0–40 Ma
Total Deformation: Thickening Plus Extension Plus Extrusion						
Thickening	64.3%	72.4%	84.5%	44%	67%	61%
Extension	24.2%	22.6%	13.3%	25.5%	18.7%	22%
Extrusion	11.5%	5%	2.2%	30.5%	14.3%	17%
Total 100%						
Resulting Percentage of Convergence Absorption						
Thickening	77.8%	90.8%	97%	37.9%	78.2%	69.8%
Extrusion	22.2%	9.2%	3%	62.1%	21.8	30.2%
Total 100%						

field be smoothed into a continuous one. Such smoothing is impossible where the changes in displacement direction and/or amplitude are large (e.g., Altyn Tagh, Sagaing faults, Himalayan thrusts).

5. Changes in Surface Areas and Integrated Deformation Budget

[66] Measuring changes in surface areas during reconstruction yields a step-by-step deformation budget, and ultimately an integrated budget for the entire collision time span. For each time step, an ''input convergence or deformation surface'' can be defined as the surface area exposed by India's backward motion. The ''output deformation surface'' of the model is the sum of the extension area, corresponding to the sum of the overlaps between blocks, of the shortening area, corresponding to the sum of the gaps between blocks (areas in which surface decrease is transformed into crustal thickening), and of the areas extruded. This latter surface area may be calculated from balancing the input and output surface area for each step of the model:

$$\Delta S_{\text{convergence}} = \left(\Delta S_{\text{shortening}} - \Delta S_{\text{extension}}\right) + \Delta S_{\text{extrusion}}.$$

[67] Two budgets are presented in Table 3. The first shows the percentage of extension, shortening and extrusion relative to the total output surface ($\Delta S_{\text{shortening}} + \Delta S_{\text{extension}} + \Delta S_{\text{extrusion}}$). The second shows the percentage of actual shortening ($\Delta S_{\text{shortening}} - \Delta S_{\text{extension}}$) and extrusion relative to the input surface ($\Delta S_{\text{convergence}}$). On Figure 9 we plot the surface areas of shortening, extension, extrusion and convergence for each time step. Even though the uncertainties involved, which are not formally included in this first backward restoration attempt, are significant, it appears that both thickening and extrusion were interplaying processes. The plot of deformation surface areas as a function of time (Figure 9) shows oscillations between extrusion and thickening, consistent with distinct deformation phases, as inferred by *Tapponnier et al.* [1986] and *Peltzer and Tapponnier* [1988].

[68] Thickening of the crust and oblique subduction of the subcrustal mantle [*Meyer et al.*, 1998; *Tapponnier et al.*, 2001] are the main processes of deformation involved between 15 Ma and the present day. Thickening absorbs ~78% of the convergence of India between 0 and 5 Ma, and extrusion only about 1/5th of it. As one goes back in time the proportion of convergence absorbed by thickening increases to ~90% between 5 Ma and 10 Ma, and to almost 100% between 10 and 15 Ma. Hence, since the mid-Miocene, as the youngest part of the Tibetan Plateau grew northeastward, the amount of extrusion, initially very small, then limited to Tibet, steadily increased to the present value. Such an increase may have been a consequence of the growth of the strike-slip faults surrounding the plateau, which propagated to reach regions located farther east. Today a significant part of the eastward motion guided by these faults past the plateau's eastern rim has begun to be transmitted to south China and to blocks in northern China, and this shows up in the overall budget. Recall however that the 5–10 Myr step includes artifacts, and that incompatibilities are not nominally dealt with in our oversimplified balance attempt.

[69] The deformation partitioning changed radically between 15 Ma and 30 Ma, when extrusion becomes the dominant process of deformation, absorbing ~62% of the surface of convergence. Such extrusion, during the Oligocene-early Miocene step, corresponds chiefly to the southeastward, wholesale escape of Indochina along the Red River-Ailao Shan shear zone.

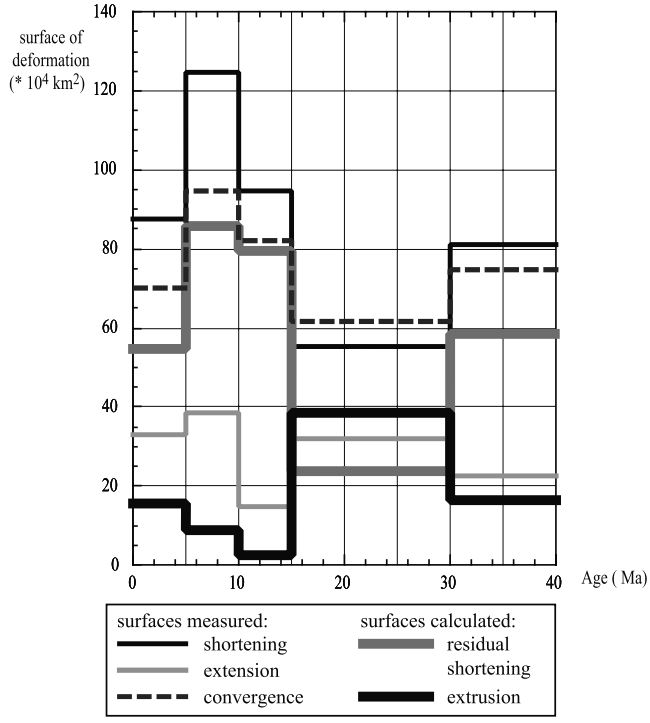


Figure 9. Deformation generated by the penetration of India as a function of time.

[70] Between 30 Ma and 40 Ma, shortening was again predominant, absorbing ~80% of the convergence surface. However, the proportion of extrusion (~20%) was significant, similar to that observed today, in large part due to the initial escape of Indochina's SW slivers along the Wang Chao and 3 Pagodas faults. Clearly, the passage from incipient to wholesale extrusion was related the 32 Ma onset of seafloor spreading in the South China Sea, which "freed" Indochina from the rest of the continent. Perhaps the birth of a new oceanic rift between the Ordos and the Yellow Sea will permit wholesale extrusion of south China in the future.

[71] Integrating the step-by-step deformation budgets shows that shortening, extension, and extrusion each accounted for an average 61%, 22%, and 17%, respectively, of the total deformation generated by the penetration of India between 0 and 40 Ma. In total, extrusion absorbed ~30% of the convergence and crustal thickening ~70%, implying that, overall, oblique subduction of the continental lithospheric mantle beneath Tibet was the principal player. Though still crude, the reconstruction quantifies variations in partitioning between thickening and extrusion during the evolution of the collision zone, and thus offers a significant improvement over the mere comparison of present-day and inferred initial positions and geometries of geological domains [e.g., *Tapponnier et al.*, 1986; *Le Pichon et al.*, 1992; *Briais et al.*, 1993].

6. Summary and Discussion

[72] Probably the main interest of our approach is that it rests on one simple hypothesis: deformation at each stage occurs along a limited number of large faults rather than on many small faults or in continuum mode. It is a first attempt to integrate such a style of deformation throughout the India-Asia collision history. By pushing reconstruction based on localized deformations to the limits, it is possible to see where the approach breaks down and to try to understand why. This may in fact be one of the most interesting outcomes of the approach. By drawing attention to the consequences of well-constrained motions on the deformation of adjacent regions, the reconstruction also yields new, testable hypotheses on the style and timing of tectonics in those regions. Because of the underconstrained nature of the problem, the technique is semiquantitative at this stage, and certain block positioning solutions chosen, nonunique. However, it permits us to deal with similarly semiquantitative geological data, and addresses continental deformation at the broad scale typical of geophysical studies.

[73] The evolutionary scenario of the India-Asia collision zone proposed is based on a synthesis of available quantitative tectonic evidence (Table 1) allowing us to solve, by continuity, for the kinematics of regions where data are insufficient. The large faults are assumed to separate lithospheric blocks that remain coherent, though not necessarily rigid at each stage. The Tarim and Ordos blocks, and much of Sunda or Indochina, for instance, are rigid today. However, other blocks deform coherently, in the sense that crustal deformation, mostly along one or several parallel boundaries, results in shrinking or expansion in one principal direction. The north Tibetan blocks, or the Himalaya, are examples of coherent shrinking. The Hebei block in north China expands coherently.

[74] The blocks are moved backward, time step-after-time step, from their present-day to their inferred positions at the onset of collision. As time unfolds back, the collision zone expands southward, shrinks westward, and the block pattern becomes simpler, in large part because less is known. Maps of the displacement fields for each time step show discrete phases of north-south shortening alternating with phases that include large east directed components of extrusion. We calculate how India's convergence with Siberia was partitioned between thickening, extension and extrusion at each step, and conclude that, overall, extrusion absorbed ≈30% of the penetration of India into Asia since 40 Ma, with great shifts from as little as 3% to as much as 60% at different epochs.

[75] The approach does not allow to test whether deformation is localized on faults or not, since this hypothesis is an a priori assumption of the model. The primary goal of the backward restoration is to assess the main acting fault pattern during each time step and its stepwise evolution during collision. The reconstruction shows that much of the deformation and motions required by quantitative geological evidence can be accommodated on a small number of large boundary faults, provided surface decrease or increase is allowed to occur along certain boundaries.

[76] Serious incompatibilities however, corresponding to gaps or overlaps that do not fit observed shortening or extension, arise at places, exposing the most conspicuous failures of the initial assumptions. They represent at least 10% of the total deformation surface. One mechanism, compatible with our a priori assumption of coherent lithospheric blocks, that minimizes misfits is large-scale block bending. This loss of torsional rigidity is the most significant element that must be added in the modeling. Bending can contribute to large shape change while requiring fairly small amounts of distributed strain. For instance, 7° of bending of the western half of the Qiangtang block (about 180 km of flexure over a distance of 1300 km) suffices to alleviate the misfit in Figure 3. Paleomagnetic data from eastern and western Tibet are consistent with such "oroclinal" bending [*Chen et al.*, 1993a, 1993b]. The most systematic, long-lived incompatibilities are observed near the eastern and western syntaxes of the Himalayan range. Even though these are rather small areas at the scale of the collision zone, our modeling implies that distributed strain is required there throughout the collision span. Likely, this is because both syntaxes are singularities in the stress field resulting from the indentation of India into Asia, and it is impossible to maintain steady state faulting around them.

[77] Although the first long-term, block reconstruction attempt presented here is crude, and becomes cruder back in time, we believe it is the only approach that can ultimately lead to complete unraveling, and insightful kinematic, hence mechanical, understanding of continental deformation. Analog modeling will likely remain plagued for some time by imperfect scaling and inadequate material properties; Numerical modeling, by its inability to deal with the birth and propagation of new discontinuities, and by difficulties in testing the smoothed results it produces against the essentially discrete, localized nature of geological strain, and the "go-stop-go" timing of tectonic phases.

Table 4. Total Displacement for Major Faults and Total Amount of Shortening for Mountain Ranges Estimated From Reconstruction

Fault	Total Displacement, km
Haiyuan	100
Kunlun west	280
Kunlun east	400
Xian Shui He	115
Dextral Red River	30
Sinistral Red River	745
Gaoligong	190
Talas Ferghana	150
Karakorum west	555
Karakorum-Zangbo	1335
Altyn Tagh southwest	460
Altyn Tagh northeast	285
Chaman	545
Sagaing	695
Tanlu	150

Mountain Range	Shortening, km
Tian Shan southwest	200
Tian Shan northeast	120
Qinling	115
Sichuan	50
Himalaya	630
Qilian	130

[78] Importantly, because a search for compatibility between motions of different types in distant places is at the core of our block reconstruction approach, it provides a rich source of new geological hypotheses to test (Table 4), which should help to set first-order goals to collect data on appropriate targets. For instance, our modeling predicts over one hundred kilometers of dextral motion on the Nicobar fault since 5 Ma, and nearly 200 km on the Gaoligong shear zone between 15 and 30 Ma (Table 4). It also predicts 115 km of shortening between south and north China, in the south Qinling belt, in the upper Miocene, and 50 km of shortening on the east side of the Sichuan basin between 30 and 15 Ma (Table 4).

[79] At this stage, the trial-and-error technique we use is imperfect. Most needed of all is a formal way of introducing uncertainties in the various inputs and outputs of the model. However, because this technique is capable of dealing with diverse types of qualitative and quantitative evidence, and of solving for self-consistency between movements and strains that are not independent over large, contiguous areas on the sphere, it should, as the data set expands, continue to improve our vision of deforming continents, whether in Asia or elsewhere.

[80] **Acknowledgments.** We thank the CNRS, IPGP, and ARCO for providing funds for this study.

References

Abdrakhmatov, K. Y., et al., Relatively recent construction of the Tian Shan inferred from GPS measurements of present-day crustal deformation rates, *Nature*, *384*, 450–453, 1996.

Allen, C. R., L. Zhuoli, Q. Hong, W. Xueze, Z. Huawei, and H. Weishi, Field study of a highly active fault zone: The Xianshuihe fault of southwestern China, *Geol. Soc. Am. Bull.*, *103*, 1178–1199, 1991.

Armijo, R., P. Tapponnier, J. L. Mercier, and H. Tonglin, Quaternary extension in southern Tibet: Field observations and tectonic implications, *J. Geophys. Res.*, *91*, 13,803–13,872, 1986.

Armijo, R., P. Tapponnier, and H. Tonglin, Late Cenozoic right-lateral strike-slip faulting in southern Tibet, *J. Geophys. Res.*, *94*, 2787–2838, 1989.

Avouac, J. P., Application des méthodes de morphologie quantitative à la néotectonique. Modèle cinématique des déformations actives en Asie Centrale, thesis, Univ. Paris VII, Paris, 1991.

Avouac, J.-P., and P. Tapponnier, Kinematic model of active deformation in central Asia, *Geophys. Res. Lett.*, *20*, 895–898, 1993.

Avouac, J. P., P. Tapponnier, M. Bai, H. You, and G. Wang, Active thrusting and folding along the northern Tian Shan and late Cenozoic rotation of the Tarim relative to Dzungaria and Kazakhstan, *J. Geophys. Res.*, *98*, 6755–6804, 1993.

Bendick, R., R. Bilham, J. Freymueller, K. Larson, and G. Yin, Geodetic evidence for a low slip rate in the Altyn Tagh fault system, *Nature*, *404*, 69–72, 2000.

Bilham, R., K. Larson, and J. Freymueller, GPS measurements of present-day convergence across the Nepal Himalaya, *Nature*, *386*, 61–64, 1997.

Briais, A., P. Patriat, and P. Tapponnier, Updated interpretation of magnetic anomalies and seafloor spreading stages in the South China Sea, implications for the Tertiary tectonics of SE Asia, *J. Geophys. Res.*, *98*, 6299–6328, 1993.

Burchfiel, B. C., Z. Chen, Y. Liu, and L. H. Royden, Tectonics of the Longmen Shan and adjacents regions, *Int. Geol. Rev.*, *108*, 1004–1021, 1996.

Burtman, V. S., S. F. Skobelev, and P. Molnar, Late Cenozoic slip on the Talas-Ferghana fault, the Tian Shan, central Asia, *Geol. Soc. Am. Bull.*, *108*, 1004–1021, 1996.

Chamot-Rooke, N., and X. Le Pichon, GPS determined eastward Sundaland motion with respect to Eurasia confirmed by earthquakes slip vectors at Sunda and Philippine trenches, *Earth Planet. Sci. Lett.*, *173*, 439–455, 1999.

Chen, Y., J. P. Cogné, V. Courtillot, P. Tapponnier, and X. Y. Zhu, Cretaceous paleomagnetic results from western Tibet and tectonic implications, *J. Geophys. Res.*, *98*, 17,981–17,999, 1993a.

Chen, Y., V. Courtillot, J. P. Cogné, J. Besse, Z. Y. Yang, and R. Enkin, The configuration of Asia prior to the collision of India: Cretaceous paleomagnetic constraints, *J. Geophys. Res.*, *98*, 21,927–21,941, 1993b.

Chen, Z., B. C. Burchfiel, Y. Liu, R. W. King, L. H. Royden, W. Tang, E. Wang, J. Zhao, and X. Zhang, Global Positioning System measurements from eastern Tibet and their implications for India/Eurasia intercontinental deformation, *J. Geophys. Res.*, *105*, 16,215–16,227, 2000.

Coward, M. P., and R. W. H. Butler, Thrust tectonics and the deep structure of the Pakistan Himalaya, *Geology*, *13*, 417–420, 1985.

DeMets, C., R. G. Gordon, D. F. Argus, and S. Stein, Effect of recent revisions to the geomagnetic reversal time scale on estimates of current plate motion, *Geophys. Res. Lett.*, *21*, 2191–2194, 1994.

Denham, C. R., and C. R. Scotese, Terra Mobilis, report, 1989.

Dewey, J. F., S. Cande, and W. C. Pitman, Tectonic evolution of the India-Eurasia collision zone, *Eclogae Geol. Helv.*, *82*, 717–734, 1989.

England, P., and G. Houseman, Finite strain calculations of continental deformation: 2. Comparison with the India-Asia collision zone, *J. Geophys. Res.*, *91*, 3664–3676, 1986.

England, P., and P. Molnar, The field of crustal velocity in Asia calculated from Quaternary rates of slip on faults, *Geophys. J. Int.*, *130*, 551–582, 1997.

Gaudemer, Y., P. Tapponnier, B. Meyer, G. Peltzer, S. Guo, Z. Chen, H. Dai, and I. Cifuentes, Partitioning of crustal slip between linked, active faults in the eastern Qilian Shan, and evidence for a major seismic gap, the "Tianzhu gap," on the western Haiyuan Fault, Gansu (China), *Geophys. J. Int.*, *120*, 599–645, 1995.

Griot, D.-A., J.-P. Montagner, and P. Tapponnier, Phase velocity structure from Rayleigh and Love waves in Tibet and its neighboring regions, *J. Geophys. Res.*, *103*, 21,215–21,232, 1998.

Gu, G., L. Ting Hong, and S. Zhen Jiliang, Catalogue of Chinese earthquakes (1831BC-1969 AD), Science Press, Beijing, China, 1989.

Guzman-Speziale, M. and J. F. Ni, Seismicity and active tectonics of the Western Sunda Arc, in *The Tectonic Evolution of Asia*, edited by A. Yin and M. Harrison, pp. 63–84, Cambridge Univ. Press, New York, 1996.

Halim, N., J. P. Cogne, Y. Chen, R. Atasiei, J. Besse, V. Courtillot, S. Gilder, J. Marcoux, and R. L. Zhao, New cretaceous and early tertiary paleomagnetic results from Xining-Lanzhou Basin, Kunlun and Qiangtang blocks, China: Implications on the geodynamic evolution of Asia, *J. Geophys. Res.*, *103*, 21,025–21,045, 1998.

Harrison, T. M., P. H. Leloup, F. J. Ryerson, P. Tapponnier, R. Lacassin, and W. Chen, Diachronous initiation of Transtension along the Ailao Shan-Red River Shear zone, Yunnan and Vietnam, in *The Tectonics of Asia*, edited by A. Yin and T. M. Harrison, pp. 208–226, Cambridge Univ. Press, New York, 1996.

Heki, K., Horizontal and vertical crustal movements from 3D very long baseline interferometry kinematic reference frame: Implication for the reversal timescale revision, *J. Geophys. Res.*, *101*, 3187–3198, 1996.

Herquel, G., P. Tapponnier, G. Wittlinger, J. Mei, and S. Danian, Teleseismic shear wave splitting and lithospheric beneath and across the Altyn Tagh fault, *Geophys. Res. Lett.*, *26*, 3225–3228, 1999.

Holt, W. E., Correlated crust and mantle strain fields in Tibet, *Geology*, *28*, 67–70, 2000.

Jaeger, J. J., V. Courtillot, and P. Tapponnier, Paleontological view of the ages of the Deccan Traps, the Cretaceous/Tertiary boundary, and the India-Asia collision, *Geology*, *17*, 316–319, 1989.

Jolivet, M., Cinematique des deformations au Nord Tibet. Thermochronologie traces de fission, modelisation analogique et etude de terrain., thesis, Univ. Montpellier II, Montpellier, France, 2000.

King, R. W., F. Shen, B. C. Burchfield, L. H. Royden, E. Wang, Z. Chen, Y. Liu, X.-Y. Zhang, J.-X. Zhao, and Y. Li, Geodetic measurement of crustal motion in southwest China, *Geology*, *25*, 179–182, 1997.

Lacassin, R., H. Maluski, P. H. Leloup, P. Tapponnier, C. Hinthong, K. Siribahakdi, S. Chuaviroj, and A. Charoenravat, Tertiary diachronic extrusion and deformation of western Indochina: Structural and $^{40}Ar/^{39}Ar$ evidence from NW Thailand, *J. Geophys. Res.*, *102*, 10,013–10,037, 1997.

Lasserre, C., Fonctionnement sismique, cinematique et histoire geologique de la faille de Haiyuan, thesis, Univ. Paris VII, Paris, 2000.

Lasserre, C., et al., Postglacial left slip rate and past occurrence of $M \geq 8$ earthquakes on the western Haiyuan fault, Gansu, China, *J. Geophys. Res.*, *104*, 17,633–17,651, 1999.

Lavé, J., and J. P. Avouac, Active folding of fluvial terraces across the Siwaliks Hills, Himalaya of central Nepal, *J. Geophys. Res.*, *105*, 5735–5770, 2000.

Lavé, J., J. P. Avouac, R. Lacassin, P. Tapponnier, and J. P. Montagner, Seismic anisotropy beneath Tibet: Evidence for eastward extrusion of the Tibetan lithosphere?, *Earth Planet. Sci. Lett.*, *140*, 83–96, 1996.

Le Dain, A. Y., P. Tapponnier, and P. Molnar, Active faults and tectonics of Burma and surrounding regions, *J. Geophys. Res.*, *89*, 453–472, 1984.

Leloup, P. H., T. M. Harrison, F. J. Ryerson, W. Chen, L. Qi, P. Tapponnier, and R. Lacassin, Structural, petrological and thermal evolution of a Tertiary ductile strike-slip shear zone, Diancang Shan, Yunnan, *J. Geophys. Res.*, *98*, 6715–6743, 1993.

Leloup, P. H., R. Lacassin, P. Tapponnier, D. Zhong, X. Liu, L. Zhang, S. Ji, and T. T. Phan, The Ailao Shan-Red River shear zone (Yunnan, China), Tertiary transform boundary of Indochina, *Tectonophysics*, *251*, 3–84, 1995.

Le Pichon, X., M. Fournier, and L. Jolivet, Kinematics, topography, shortening, and extrusion in the India-Eurasia collision, *Tectonics*, *11*, 1085–1098, 1992.

Lesne, O., E. Calais, J. Déverchère, C. Petit, V. Sankov, and K. Levi, Active deformation in the Baikal rift zone, Siberia, from GPS measurements, sismotectonic analysis, and finite element modeling, paper presented at EUG 9, Strasbourg, France, 1997.

Liu, Q., Paléoclimat et contraintes chronologiques sur les mouvements récents dans l'Ouest du Tibet: Failles du Karakorum et de Longmu Co-Gozha Co, lacs en pull-apart de Longmu Co et de Sumxi Co, thesis, Univ. Paris VII, Paris, 1993.

Matte, P., M. Mattauer, J. M. Oliver, and D. A. Griot, Continental subductions beneath Tibet and the Himalayan orogeny: A review, *Terra Nova*, *9*, 264–270, 1997.

McCaffrey, R., and J. Nabelek, Role of oblique convergence in the active deformation of the Himalaya and southern Tibet plateau, *Geology*, *26*, 691–694, 1998.

McClusky, S. M., et al., Global Positioning System constraints on plate kinematics and dynamics in the eastern Mediterranean and Caucasus, *J. Geophys. Res.*, *105*, 5695–5719, 2000.

McNamara, D., T. J. Owens, P. G. Silver, and F. T. Wu, Shear wave anisotropy beneath the Tibetan Plateau, *J. Geophys. Res.*, *99*, 13,655–13,665, 1994.

Mériaux, A. S., Détermination par datation cosmogénique des variations de la vitesse de glissement sur la faille de l'Altyn Tagh depuis 100ka, thesis, Univ. Paris VII, Paris, 2002.

Mériaux, A. S., and P. Tapponnier, Application of cosmogenic ^{10}Be and ^{26}Al dating to Neotectonics of the Altyn Tagh fault in central Asia (Gansu, China), *Eos Trans. AGU*, *78*(46), Fall Meet. Suppl., F173, 1997.

Mériaux, A.-S., F. J. Ryerson, P. Tapponnier, J. Vanderwoerd, R. Finkel, M. Caffee, C. Lasserre, X. Xu, H. Li, and Z. Xu, Fast extrusion of the Tibet Plateau: A 3 cm/yr, 100 kyr slip-rate on the Altyn Tagh Fault, *Eos Trans. AGU*, *81*(48), Fall Meet. Suppl., Abstract T62D-07, 2000.

Metivier, F., Y. Gaudemer, P. Tapponnier, and M. Klein, Mass accumulation rates in Asia during the Cenozoic, *Geophys. J. Int.*, *137*, 280–318, 1999.

Meyer, B., P. Tapponnier, L. Bourjot, F. Metivier, Y. Gaudemer, G. Peltzer, G. Shunmin, and C. Zhitai, Mechanisms of active crustal thickening in Gansu-Qinghai, and oblique, strike-slip controlled, northeastward growth of the Tibet Plateau, *Geophys. J. Int.*, *133*, 1–47, 1998.

Michel, G. W., M. Becker, D. Angermann, C. Reigber, and E. Reinhart, Crustal motion in E- and SE-Asia from GPS measurements, *Earth Planets Space*, *52*, 713–720, 2000.

Molnar, P., and H. Lyon-Caen, Fault plane solution of earthquake and active tectonics of the Tibetan plateau and its margins, *Geophys. J. Int.*, *99*, 123–153, 1989.

Molnar, P., and P. Tapponnier, Cenozoic tectonics of Asia: Effects of a continental collision, *Science*, *189*, 419–426, 1975.

Molnar, P., and P. Tapponnier, Active tectonics of Tibet, *J. Geophys. Res.*, *83*, 5361–5375, 1978.

Molnar, P., F. Parco-Casas, and J. Stock, The Cenozoic and Late Cretaceous evolution of the Indian Ocean Basin: Uncertainties in the reconstructed positions of the Indian, African and Antarctic plates, *Basin Res.*, *1*, 23–40, 1988.

Patriat, P., and J. Achache, India-Eurasia collision chronology has implications for crustal shortening and driving mechanism of plates, *Nature*, *311*, 615–621, 1984.

Peltzer, G., and F. Saucier, Present-day kinematics of Asia, derived from geologic fault rates, *J. Geophys. Res.*, *101*, 27,943–27,956, 1996.

Peltzer, G., and P. Tapponnier, Formation and evolution of strike-slip faults, rifts, and basins during India-Asia collision: An experimental approach, *J. Geophys. Res.*, *93*, 15,085–15,117, 1988.

Peltzer, G., P. Tapponnier, Z. Zhang, and Z. Q. Xu, Neogene and quaternary faulting in and along the Qinling shan, *Nature*, *317*, 500–505, 1985.

Peltzer, G., P. Tapponnier, and R. Armijo, Magnitude of late Quaternary left-lateral displacements along the northern edge of Tibet, *Science*, *246*, 1285–1289, 1989.

Ratschbacher, L., W. Frish, and G. Liu, Distributed deformation in the southern and western Tibet during and after the India-Asia collision, *J. Geophys. Res.*, *99*, 19,917–19,945, 1994.

Replumaz, A., R. Lacassin, P. Tapponnier, and P. H. Leloup, Large river offsets and Plio-Quaternary dextral slip rate on the Red River fault (Yunnan, China), *J. Geophys. Res.*, *106*, 819–836, 2001.

Ritz, J. F., E. T. Brown, B. D. L. Dummy, H. Philip, A. Schlupp, G. M. Raisbeck, F. Yiou, and B. Enkhtuvshin, Slip rates along active faults estimated with cosmic-ray-exposure dates: Application to the Bogd fault, Gobi-Altai, Mongolia, *Geology*, *23*, 1019–1022, 1995.

Roger, F., P. Tapponnier, N. Arnaud, U. Scharer, M. Brunel, Z. Xu, and J. Yang, An Eocene magmatic belt across central Tibet: Mantle subduction triggered by the Indian collision?, *Terra Nova*, *12*, 102–108, 2000.

Schärer, U., P. Tapponnier, R. Lacassin, P. H. Leloup, D. Zhong, and S. Ji, Intraplate tectonics in Asia: A precise age for large-scale Miocene movement along the Ailao Shan-Red River shear zone, China, *Earth Planet. Sci. Lett.*, *97*, 65–77, 1990.

Shen, Z. K., C. Zhao, A. Yin, Y. Li, D. D. Jackson, P. Fanga, and D. Dong, Contemporary crustal deformation in east Asia constrained by Global Positioning System measurements, *J. Geophys. Res.*, *105*, 5721–5734, 2000.

Shen, Z. K., M. Wang, Y. Li, D. D. Jackson, A. Yin, D. Dong, and P. Fang, Crustal deformation along the Altyn Tagh fault system, western China, from GPS, *J. Geophys. Res.*, *106*, 30,607–30,621, 2001.

Sieh, K., and D. Natawidjaja, Neotectonics of the Sumatran fault, Indonesia, *J. Geophys. Res.*, *105*, 28,295–28,326, 2000.

Tapponnier, P., and P. Molnar, Active faulting and tectonics in China, *J. Geophys. Res.*, *82*, 2905–2930, 1977.

Tapponnier, P., and P. Molnar, Active faulting and Cenozoic tectonics of the Tian Shan, Mongolie, and Baikal regions, *J. Geophys. Res.*, *84*, 3425–3459, 1979.

Tapponnier, P., G. Peltzer, R. Armijo, A.-Y. Le Dain, and P. Cobbold, Propagating extrusion tectonics in Asia: New insights from simple experiments with plasticine, *Geology*, *10*, 611–616, 1982.

Tapponnier, P., G. Peltzer, R. Armijo, On the mechanics of the collision between India and Asia, in *Collision Tectonics*, edited by J. G. Ramsay, M. P. Coward, and A. C. Ries, *Geol. Soc. Spec. Publ.*, *19*, 115–157, 1986.

Tapponnier, P., R. Lacassin, P. H. Leloup, U. Schärer, D. Zhong, X. Liu, S. Ji, L. Zhang, and J. Zhong, The Ailao Shan/red River metamorphic belt: Tertiary left-lateral shear between Indochina and south China, *Nature*, *343*, 431–437, 1990.

Tapponnier, P., X. Zhiding, F. Roger, B. Meyer, N. Arnaud, G. Wittlinger, and Y. Jingsui, Oblique stepwise rise and growth of the Tibet Plateau, *Science*, *294*, 1671–1677, 2001.

Van Der Woerd, J., Couplage cinématique entre décrochements et chevauchements actifs dans le Nord du Tibet: Croissance du plateau du Tibétain., thesis, Univ. Paris VII, Paris, 1998.

Van Der Woerd, J., F. J. Ryerson, P. Tapponnier, Y. Gaudemer, R. Finkel, A. S. Mériaux, M. Caffee, Z. Guoguang, and H. Qunlu, Holocene left-slip rate determined by cosmogenic surface dating on the Xidatan segment of the Kunlun fault (Qinghai, China), *Geology*, *26*, 695–698, 1998.

Van Der Woerd, J., F. J. Ryerson, P. Tapponnier, A. S. Mériaux, Y. Gaudemer, B. Meyer, R. Finkel, M. Caffee, G. G. Zhao, and Z. Q. Xu, Uniform Slip-Rate along the Kunlun Fault: Implications for seismic behaviour and large-scale tectonics, *Geophys. Res. Lett.*, *27*, 2353–2356, 2000.

Vilotte, J. P., R. Madariaga, M. Daignières, and O. Zienkiewicz, Numerical study of continental collision: Influence of buoyancy forces and an initial stiff inclusion, *Geophys. J. R. Astron. Soc.*, *84*, 279–310, 1986.

Walpersdorf, A., C. Vigny, P. Manurung, C. Subaraya, and S. Sutisna, Determining the Sula block kinematics in the triple junction area in Indonesia by GPS, *Geophys. J. Int.*, *135*, 351–361, 1998.

Wang, E., B. C. Burchfiel, L. H. Royden, L. Chen, J. Chen, W. Li, and Z. Chen, Late Cenozoic Xianshuihe-Xiaojiang, Red River, and Dali fault systems of southwestern Sichuan and central Yunnan, China, *Spec. Pap. Geol. Soc. Am*., *327*, 108 pp., 1998.

Wang, Q., et al., Present-day crustal deformation in China constrained by Global Positioning system measurements, *Science*, *294*, 574–577, 2001.

Wilson, P., et al., Study provides data on active plate tectonics in Southeast Asia region, *Eos Trans. AGU*, *79*, 545, 548–549, 1998.

Wittlinger, G., P. Tapponnier, G. Poupinet, J. Mei, S. Danian, G. Herquel, and F. Masson, Tomographic evidence for localized shear along the Altyn Tagh fault, *Science*, *282*, 74–76, 1998.

Yang, Z., and J. Besse, Paleomagnetic study of Permian and Mesozoic sedimentary rocks from Northern Thailand supports the extrusion model for Indochina, *Earth Planet. Sci. Lett.*, *117*, 525–552, 1993.

Yin, A., Mode of Cenozoic east-west extension in Tibet suggesting a common origin of rifts in Asia during the Indo-Asian collision, *J. Geophys. Res.*, *105*, 21,745–21,759, 2000.

Yin, A., T. M. Harrison, M. A. Murphy, M. Grove, S. Nie, F. J. Ryerson, W. X. Feng, and C. Z. Le, Tertiary deformation history of southeastern and southwestern Tibet during the Indo-Asian collision, *Geol. Soc. Am. Bull.*, *111*, 1644–1664, 1999.

Zhang, Y., Tectonique Cenozoique en Chine du Nord: Extension autour de l'Ordos et décrochements sur le système de failles des Qinling et de Tanlu, thesis, Univ. Paris XI, Paris, 1994.

Zhong, D. and L. Ding, The Tertiary Gaoligong intra-continental strike-slip fault and its associated extensional structure in western Yunnan, China, report, Lab. of Lithospheric Tectonic Evol., Inst. of Geol., Acad. Sin., Beijing, 1991.

A. Replumaz, Université Claude Bernard-Lyon 1, UMR CNRS 5570 Bât. géode, Laboratoire Dynamique de la Lithosphère, 2 rue R. Dubois, F-69622 Villeurbanne cedex, France. (anne.replumaz@univ-lyon1.fr)

P. Tapponnier, Laboratoire de Tectonique, Mécanique de la Lithosphère, UMR 7578 Centre National de la Recherche Scientifique, Institut de Physique du Globe de Paris, 4 place Jussieu, F-75252 Paris Cedex 05, France. (tappon@ipgp.jussieu.fr)